Mon. Not. R. Astron. Soc. **318**, 665–680 (2000)

Statistical characteristics of simulated walls

M. Demiański,[1,2] A. G. Doroshkevich,[3,4] V. Müller[5] and V. Turchaninov[4]

[1]*Institute of Theoretical Physics, University of Warsaw, 00-681 Warsaw, Poland*
[2]*Department of Astronomy, Williams College, Williamstown, MA 01267, USA*
[3]*Theoretical Astrophysics Center, Juliane Maries Vej 30, DK-2100 Copenhagen Ø, Denmark*
[4]*Keldysh Institute of Applied Mathematics, Russian Academy of Sciences, 125047 Moscow, Russia*
[5]*Astrophysikalisches Institute Potsdam, An der Sternwarte 16, D-14482 Potsdam, Germany*

Accepted 2000 May 1. Received 2000 March 17; in original form 1999 July 14

ABSTRACT

The large-scale matter distribution in three different simulations of CDM models is investigated and compared with corresponding results of the Zel'dovich theory of non-linear gravitational instability. We show that the basic characteristics of wall-like structure elements are well described by this theory, and that they can be expressed by the cosmological parameters and a few spectral moments of the perturbation spectrum. Therefore the characteristics of such elements provide reasonable estimates of these parameters. We show that the compressed matter is relaxed and gravitationally confined and manifests itself in the existence of walls as (quasi-)stationary structure elements with a lifetime restricted by their disruption into high-density clouds.

The matter distribution is investigated in both real and redshift spaces. In both cases almost the same particles form the walls, and we estimate differences in corresponding wall characteristics. The same methods are applied to several mock catalogues of 'galaxies', which allows us to characterize a large-scale bias between the spatial distribution of dark matter and of simulated 'galaxies'.

Key words: galaxies: clusters: general – cosmology: theory – dark matter – large-scale structure of Universe.

1 INTRODUCTION

Over the past decade immense progress has been achieved in the investigation of the large-scale matter distribution. Now the galaxy distribution is studied up to redshift $z \sim 3$ (Steidel et al. 1996). At smaller redshifts the analysis of rich galaxy surveys with an effective depth $\sim(200–400)\,h^{-1}$ Mpc, such as the Durham/UKST Galaxy Redshift Survey (Ratcliffe et al. 1996) and the Las Campanas Redshift Survey (Shectman et al. 1996), has established the existence of wall-like structure elements as a typical phenomenon in the visible galaxy distribution incorporating ~40–50 per cent of galaxies (Doroshkevich et al. 1996, hereafter LCRS1; Doroshkevich et al. 1999a, hereafter LCRS2; Doroshkevich et al. 2000, hereafter DURS). The wall-like structure elements with a typical diameter $\sim(30–50)\,h^{-1}$ Mpc surround low-density regions with a similar typical diameter $\sim(50–70)\,h^{-1}$ Mpc. Within the wall-like structures, the observed galaxy distribution is also inhomogeneous (see, e.g., fig. 5 of Ramella, Geller & Huchra 1992), and galaxies are concentrated in high-density clumps and filaments.

The galaxies occupying low-density regions are concentrated within a random network of filaments. Filaments incorporate ~50 per cent of galaxies, and are clearly seen in many redshift surveys (see, e.g., de Lapparent, Geller & Huchra 1988). These results extend the range of investigated scales in the galaxy distribution up to $\sim 100\,h^{-1}$ Mpc. Further progress in the study of the observed large-scale galaxy distribution could be reached with the 2dF redshift survey (Cannon 1998; Colless 1998) and the Sloan Digital Sky Survey (Loveday & Pier 1998).

The formation and evolution of structure on large scales are investigated in numerous simulations (see, e.g., Cole et al. 1997, 1998, Governato et al. 1998, Jenkins et al. 1998, Müller et al. 1998 and Doroshkevich et al. 1999b, hereafter DMRT). These simulations are performed in large boxes ($\sim 350–500\,h^{-1}$ Mpc), and reproduce the main properties of the observed large-scale matter distribution. In particular, they confirm formation of large wall-like matter condensations due to a non-linear anisotropic matter compression on a typical scale $\sim(20–30)\,h^{-1}$ Mpc, which is about one-half of the typical wall separation.

The statistical characteristics of wall formation are described by an approximate theoretical model (Lee & Shandarin 1998; Demiański & Doroshkevich 1999a, 1999b, hereafter DD99) based on the Zel'dovich non-linear theory of gravitational instability (Zel'dovich 1970, 1978; Shandarin & Zel'dovich 1989). This approach relates the structure parameters with the main parameters of the underlying cosmological scenario and the

initial power spectrum of density perturbations. The impact of large-scale perturbations is found to be important throughout all evolutionary stages, and some statistical characteristics of structure elements–filaments and walls formed in the course of non-linear evolution–are directly connected with the parameters of these perturbations. Another theoretical model of large-scale structure formation was discussed in Bond, Kofman & Pogosyan (1996).

The simulated large-scale matter distribution does not exactly reproduce the theoretical expectations due to the influence of some essential factors, the most important ones being the small-scale clustering and relaxation of compressed matter, and the large-scale matter flow within sheet-like structure elements. Thus, compression of matter along one of the transversal directions transforms sheet-like elements into filaments, while expansion of matter in both transversal directions results in the erosion of pancakes. The disruption of walls and the small-scale clustering of compressed matter substantially accelerate the relaxation and are responsible for strong matter concentration within walls. This is apparent from the isotropy of velocity dispersion within walls noticed in DMRT.

The combined influence of these (and other) factors complicates the statistical description of the large-scale matter distribution at late evolutionary stages, which is typical for the final evolutionary stages of the standard *COBE*-normalized CDM (SCDM) model with $\Omega_{\rm m} = 1$. For low-density models, such as the open CDM (OCDM) model and the ΛCDM model with $\Omega_\Lambda > \Omega_{\rm m}$, the situation is not so complex, and some statistical characteristics of structure can be successfully compared with the approximate theoretical expectations.

The investigation of wall-like massive structure elements is more promising in this respect, because walls represent the first step in the process of structure formation, and therefore hold more information about characteristics of the initial matter flow. Such walls are observed as superclusters of galaxies similar to the Great Wall (de Lapparent et al. 1988) and the Pisces-Perseus supercluster (Giovanelli & Haynes 1993). In simulations such wall-like structure elements are also easily identified because of their relatively high overdensity. Samples of such elements were investigated in DMRT and LCRS2. The connection between the properties of walls and the amplitude and spectrum of initial perturbations was discussed in DD99, and some of these results can be compared with measured properties of simulated wall-like structure elements. Examples considered in DD99 and DMRT had a rather illustrative character, but they seem to be quite promising.

Here we will compare more accurately some of the expected and measured characteristics of wall-like matter condensations. We concentrate our attention on the physical aspects of the formation and evolution of the large-scale matter distribution in order to better understand these processes and the phenomenon of wall-like matter condensations. Both theoretical and numerical estimates are inevitably approximate, but nevertheless such comparison allows us to test the theoretical conclusions, to reveal and illustrate the influence of essential factors mentioned above, and to examine the abilities of statistical methods used to describe the large-scale matter distribution.

These methods allow us to reveal, in particular, some differences in characteristics of the large-scale matter distribution in real and redshift spaces. Various aspects of this problem have been widely discussed during the past decade (see, e.g., Kaiser 1987, McGill 1990a, Davis, Miller & White 1997, Hamilton 1998, Melott et al. 1998, Hui, Kofman & Shandarin 2000 and Tadros et al. 1999). Here we show that the differences between characteristics of walls in real and redshift spaces depend on the basic cosmological model and increase during the cosmic evolution. Characteristics of walls in real and redshift spaces are almost identical for the low-density models, but they differ more strongly for the SCDM model.

We do not discuss the application of these methods to the observed galaxy catalogues, which is a much harder problem, due to the strong influence of selection effects and other factors. We will consider this problem in the future.

This paper is organized as follows. In Section 2 the basic notations are introduced. In Section 3 the statistical characteristics of wall-like structure elements in the Zel'dovich theory are presented. In Section 4 we consider the methods used to measure the required characteristics of matter distribution. Our results are presented in Sections 5 and 6, where they are also compared with the theoretical expectations. Section 7 contains a summary and a short discussion of our main results. Some technical details are given in Appendix A.

2 STATISTICAL CHARACTERISTICS OF LARGE-SCALE STRUCTURE

It is generally recognized that the formation of observed large-scale structure is driven by the middle part of the power spectrum, $p(k)$, with $0.2\,h\,{\rm Mpc}^{-1} \geq k \geq 0.01\,h\,{\rm Mpc}^{-1}$ (k is the comoving wavenumber), and it is weakly sensitive to the small- and large-scale perturbations. In many publications authors use an artificial smoothing of the spectrum to describe this process (see, e.g., Bardeen et al. 1986, hereafter BBKS, and Coles et al. 1993). However, as was shown in DD99, it is possible to avoid this artificial smoothing if the process of structure formation is described in terms of the displacement, $S_i(\boldsymbol{q})$, and the velocity rather than the density field.

Indeed, in contrast with the density field, the statistical characteristics of displacements are weakly sensitive to the small- and large-scale perturbations, and are reasonably well described by the middle part of the initial power spectrum. Even the strong non-linear matter clustering does not significantly influence the main characteristics of displacements, and so such (approximate) description of structure holds during a long period of structure evolution. Of course, this approach cannot describe the formation of gravitationally confined walls and their disruption into a system of high-density clouds.

Bearing in mind these comments, we will describe the structure parameters using characteristics directly connected with the displacement. One of them is the large-scale amplitude of perturbations measured by the dispersion of displacements,

$$\sigma_{\rm s}^2(z) = \frac{1}{2\pi^2}\int_0^\infty p(z,k)\,{\rm d}k, \tag{2.1}$$

Another convenient parameter is the coherent length of the displacement and velocity fields, $l_{\rm v}$, expressed through the moment m_{-2} of the initial power spectrum, $p(k)$. A suitably defined coherent length $l_{\rm v}$ provides simple expressions for the correlation functions of these fields and the basic characteristics of the large-scale structure (DD99 and Section 3).

2.1 The Zel'dovich approximation

The Zel'dovich theory connects the Eulerian, r_i, and the

Lagrangian, q_i, coordinates of fluid elements (particles) by the expressions

$$r_i = (1+z)^{-1}[q_i - B(z)S_i(\boldsymbol{q})], \qquad (2.2)$$
$$S_i(\boldsymbol{q}) = \partial\Phi(\boldsymbol{q})/\partial q_i,$$

where z denotes the redshift, $B(z)$ describes the growth of perturbations in the linear theory, and the random vector S_i or the random potential Φ characterize the spatial distribution of perturbations. The Lagrangian coordinates of a particle, q_i, are its unperturbed comoving coordinates.

The velocity of a particle can be found from (2.2) as

$$u_i(\boldsymbol{q},z) = \frac{\mathrm{d}r_i}{\mathrm{d}t} = \frac{H(z)}{1+z}[q_i - (1+\beta)B(z)S_i(\boldsymbol{q})],$$
$$\beta(z) = -\frac{1+z}{B}\frac{\mathrm{d}B(z)}{\mathrm{d}z}, \qquad (2.3)$$
$$H(z) = H_0\sqrt{\Omega_\mathrm{m}(1+z)^3 + (1-\Omega_\mathrm{m}-\Omega_\Lambda)(1+z)^2 + \Omega_\Lambda},$$

where H is the Hubble constant ($H_0 = 100\,h\,\mathrm{km\,s^{-1}\,Mpc^{-1}}$). Analytical fits for the functions $B(z)$ and $\beta(z)$ were given in DD99. Approximately, at $z \ll 1$, we have

$$B(0) = 1, \quad \beta(0) \approx \frac{2.3\Omega_\mathrm{m}}{1+1.3\Omega_\mathrm{m}}. \qquad (2.4)$$

2.2 Main structure characteristics for the CDM-like power spectrum

The standard CDM-like power spectrum with a Harrison–Zel'dovich large-scale asymptote,

$$p_\mathrm{cdm}(k) = A(z)kT^2(k/k_0), \quad k_0 = \Gamma\,h\,\mathrm{Mpc}^{-1}, \qquad (5)$$
$$\Gamma = \sqrt{\frac{1.7\rho_\gamma}{\rho_\mathrm{rel}}}\Omega_\mathrm{m}h,$$

can be taken as a reasonable approximation of the initial power spectrum used in the Zel'dovich theory. Here $A(z)$ is the amplitude of perturbations, $T(x)$ is a transfer function, and ρ_γ and ρ_rel are the densities of CMB photons and relativistic particles (photons, neutrinos, etc.). For this spectrum the parameters l_v and σ_s are expressed through the spectral moments, m_j, as follows:

$$l_v^{-2} = \int_0^\infty kT^2(k/k_0)\,\mathrm{d}k = m_{-2}k_0^2, \qquad (2.6)$$
$$\sigma_s^2 \equiv \frac{1}{2\pi^2}\int_0^\infty p_\mathrm{cdm}(k)\,\mathrm{d}k = \frac{A(z)}{2\pi^2}k_0^2 m_{-2} = \frac{A(z)}{2\pi^2 l_v^2},$$
$$m_j = \int_0^\infty x^{3+j}T^2(x)\,\mathrm{d}x, \quad m_{-2} = \int_0^\infty xT^2(x)\,\mathrm{d}x.$$

For the CDM transfer function (BBKS) $m_{-2} = 0.023$, the expressions for the scale l_v and the characteristic masses of dark matter (DM) and baryonic components associated with the scale l_v can be written more explicitly as

$$l_\mathrm{v} \approx \frac{6.6}{\Gamma}\sqrt{\frac{0.023}{m_{-2}}}h^{-1}\,\mathrm{Mpc}, \qquad (2.7)$$
$$M_\mathrm{v} = \frac{4\pi}{3}\langle\rho\rangle l_v^3 \approx \frac{2\times10^{14}\,\mathrm{M}_\odot}{\Gamma^2h^2}, \quad M_b^{(0)} = \frac{\Omega_b}{\Omega_\mathrm{m}}M_\mathrm{v}.$$

Here Ω_b is the dimensionless mean density of the baryonic component. The same characteristic scale l_v, as given by (2.7), can be used for the structure description, as long as the Zel'dovich theory can be applied.

More details can be found in DD99. The same approach can be used for other power spectra as well.

2.3 The amplitude of large-scale perturbations

The large-scale amplitude of perturbation as measured by $A(z)$ in (2.5) and σ_s (2.1) can be successfully used to describe the structure evolution in the framework of the Zel'dovich theory. As was shown in DD99, it is convenient to use–together with σ_s–an effective dimensionless 'time', $\tau(z, \Omega_\mathrm{m}, h)$,

$$\tau(z) = \frac{\sigma_\mathrm{s}}{\sqrt{3}l_\mathrm{v}}, \qquad (2.8)$$

which is proportional to the large-scale amplitude of perturbations and suitably describes the evolutionary stage reached in the model. This 'time' is similar to that used in the adhesion model (Shandarin & Zel'dovich 1989).

As was noticed in DD99, the structure evolution shows strong features of self-similarity, and is described by universal expressions depending on the dimensionless variables $\boldsymbol{q}/l_\mathrm{v}$ and τ. This is a direct consequence of the Zel'dovich approximation.

The 'time' τ can be measured by different methods, some of which are discussed below. It is sensitive to the sample under investigation and to the method of measurement. It can be used to quantify bias between spatial distributions of different objects, such as, for example, large-scale bias between distributions of galaxies and the DM component.

The quadrupole component of the CMB anisotropy, T_Q, the variance of density in a sphere with radius $8\,h^{-1}\,\mathrm{Mpc}$, σ_8, and the velocity dispersion, σ_vel, are the more often used characteristics of the large-scale amplitude. All these characteristics are proportional to each other, but their dependence on Ω_m and h is different, and they are sensitive to matter distribution on different scales. Thus the quadrupole component of CMB anisotropy characterizes the perturbations on scales comparable with the horizon, while the values σ_vel and σ_8 are more sensitive to the matter distribution on moderate and small scales.

The connection of these characteristics with σ_s and τ can be summarized as follows.

(i) Using the fits for the CMB anisotropy proposed by Bunn & White (1997), we obtain for the flat ΛCDM and open OCDM models

$$\tau_T \approx 2.73\,h^2\Omega_m^{1.2}\left(\frac{m_{-2}}{0.023}\frac{T_\mathrm{Q}}{20\,\mu\mathrm{K}}\right), \quad \Omega_\Lambda = 1-\Omega_\mathrm{m}, \qquad (2.9)$$
$$\tau_T \approx 2.73\,h^2\Omega_m^{1.65-0.19\ln\Omega_\mathrm{m}}\left(\frac{m_{-2}}{0.023}\frac{T_\mathrm{Q}}{20\,\mu\mathrm{K}}\right), \quad \Omega_\Lambda = 0,$$

where τ_T denotes the amplitude of large-scale perturbations, τ, measured by the CMB anisotropy. These estimates depend on the spectral moment m_{-2} only, which is very stable and does not change during the considered period of evolution. However, the estimates should be corrected if a possible contribution of gravitational waves is taken into account.

(ii) The amplitude of perturbations, σ_s and τ, can be directly expressed through the two-point autocorrelation function as follows:

$$\sigma_s^2 = \lim_{r\to\infty}\int_0^r \mathrm{d}x\left(1-\frac{x}{r}\right)x\xi(x), \qquad (2.10)$$

and for the autocorrelation function $\xi(r)$, approximated by the power law

$$\xi(r) = (r_0/r)^{\gamma}, \quad r \le r_{\xi}, \tag{2.11}$$

we have

$$\sigma_s^2(r_{\xi}) \approx \frac{r_{\xi}^{2-\gamma} r_0^{\gamma}}{(2-\gamma)(3-\gamma)}, \quad \tau_{\xi} = \frac{\sigma_s(r_{\xi})}{\sqrt{3} l_v}. \tag{2.12}$$

Here r_{ξ} is the first zero-point of the autocorrelation function, and τ_{ξ} denotes the amplitude τ measured by this function. The parameter r_{ξ} is usually found with small precision, but for $\gamma \approx 1.5$–1.7, $1 - \gamma/2 \approx 0.25$–$0.15$ even some variations of r_{ξ} do not change significantly the final estimate of τ.

(iii) The parameter σ_8 can be also expressed through the two-point autocorrelation function, $\xi(r)$ (Peebles 1993), and for $\xi(r)$ approximated by a power law (2.11) we have

$$\sigma_8^2 = \frac{72}{(3-\gamma)(4-\gamma)(6-\gamma)} \left(\frac{r_0}{16\, h^{-1}\,\mathrm{Mpc}} \right)^{\gamma}, \tag{2.13}$$

$$\sigma_s^2 \approx \sigma_8^2 (8\, h^{-1}\,\mathrm{Mpc})^2 \frac{(4-\gamma)(6-\gamma)}{18(2-\gamma)} \left(\frac{r_{\xi}}{16\, h^{-1}\,\mathrm{Mpc}} \right)^{2-\gamma},$$

$$\tau_8 = \sigma_8 \Gamma \sqrt{\frac{(4-\gamma)(6-\gamma)}{36.75(2-\gamma)}} \left(\frac{r_{\xi}}{16\, h^{-1}\,\mathrm{Mpc}} \right)^{\frac{2-\gamma}{2}}. \tag{2.14}$$

(iv) The dispersion of the peculiar velocity of particles at small redshifts, $z \sim 0$, can be written as in the linear theory (DD99)

$$\sigma_{\mathrm{vel}} = u_0 \sqrt{3} \tau, \quad u_0 = l_v H_0 \beta \approx \frac{\Omega_m}{\Gamma} \frac{1535\,\mathrm{km\,s^{-1}}}{1 + 1.3\Omega_m}, \tag{2.15}$$

and for τ we obtain the independent estimate

$$\tau_{\mathrm{vel}} = \frac{\sigma_{\mathrm{vel}}}{\sqrt{3} u_0}. \tag{2.16}$$

Here τ_{vel} denotes the amplitude τ measured by the velocity dispersion. σ_{vel} takes into account also the high velocities generated by the gravitational compression of matter (in particular, within clusters of galaxies), and so it actually gives an upper limit of the amplitude.

3 STATISTICAL CHARACTERISTICS OF WALLS IN THE ZEL'DOVICH THEORY

In both observed and simulated catalogues, at small redshifts, the wall-like structure elements accumulate ~50 per cent of galaxies and form the skeleton of large-scale structure. So, investigation of the characteristics of these elements is important in itself. It allows us also to obtain information about processes of non-linear structure evolution. In particular, we can find two independent measures of the large-scale amplitude, τ. As walls represent the first step of the large-scale non-linear matter compression, their characteristics can be compared with predictions of the Zel'dovich theory.

In this section we will consider five characteristics of walls, namely, the surface density of walls, m_w, defined as the amount of matter per unit of wall surface, for example, per $h^{-2}\,\mathrm{Mpc}^2$, the thickness of walls, h_w, the wall separation, D_{sep}, the velocity dispersion of matter compressed within walls, w_w, and the dispersion of wall velocities, σ_v. All these characteristics can be derived from the Zel'dovich theory (DD99), and can be found for simulated point distributions as well.

3.1 Formation of walls

Following DD99, we will consider the intersection of two fluid particles with Lagrangian coordinates $\boldsymbol{q}_1$ and $\boldsymbol{q}_2$ as the formation of a wall (Zel'dovich pancake) with the surface density $m_w = \langle n_p \rangle |\boldsymbol{q}_1 - \boldsymbol{q}_2|$, where $\langle n_p \rangle$ is the mean particles density in the sample. In Zel'dovich theory, statistical characteristics of such walls are described by the initial power spectrum (2.5), and can be expressed through the characteristic scale, l_v, the surface density of wall, m_w, or dimensionless surface density, $q_w = m_w/l_v/\langle n_p \rangle$, and the 'time', τ, introduced in Section 2. To do this, the structure functions of the initial power spectrum can be used. For the standard SDM-like power spectrum (2.5) with the BBKS transfer function these functions were introduced in DD99.

Naturally, the theoretical considerations describe the idealized model of structure evolution. Thus it uses the rigid wall boundary, although in reality such boundaries are always blurred. Another important factor is the compression and expansion of pancakes in transverse directions. These motions transform pancakes into filaments and/or lead to the dissipation of poor pancakes. They are not so important for rich walls, but can change the wall surface density by a factor of 1.3–1.5. The small-scale clustering and relaxation of matter also distorts the measured characteristics of walls with respect to theoretical expectations.

These factors distort the actual power spectrum with respect to the one used and introduce differences between the expected and actually measured parameters of walls, which however cannot be evaluated a priori. The actual power and limitations of this approach must first be tested with *N*-body simulations.

3.2 Wall properties in real space

3.2.1 Surface density of walls

The most fundamental characteristic of walls is the surface density, m_w. The approximate expression for the probability distribution function (PDF) of the pancakes surface density, m_w, defined as above, has been obtained in DD99 in the same manner as the well-known Press–Schechter mass function. It characterizes the process of one-dimensional (1D) matter compression and formation of wall-like pancakes as described by the Zel'dovich theory.

For Gaussian initial perturbations and the standard CDM-like power spectrum with the BBKS transfer function, it can be written as follows:

$$N_m = \frac{1}{\sqrt{2\pi}\tau_m} \frac{1}{\sqrt{q_w}} \exp\left(-\frac{q_w}{8\tau_m^2} \right) \mathrm{erf}\left(\sqrt{\frac{q_w}{8\tau_m^2}} \right), \tag{3.1}$$

$$q_w = \frac{m_w}{l_v \langle n_p \rangle} = \frac{|\boldsymbol{q}_1 - \boldsymbol{q}_2|}{l_v}, \quad \int_0^{\infty} N_m(q_w)\, \mathrm{d}q_w = 1,$$

$$\langle q_w \rangle = \int_0^{\infty} q_w N_m(q_w)\, \mathrm{d}q_w = 8(0.5 + 1/\pi)\tau_m^2 \approx 6.55\tau_m^2,$$

$$\langle q_w^2 \rangle = \int_0^{\infty} q_w^2 N_m(q_w)\, \mathrm{d}q_w = 128(0.375 + 1/\pi)\tau_m^4 \approx 887\tau_m^4,$$

where $\langle n_p \rangle$ is the mean particle density in the sample, l_v is defined by (2.7), τ_m characterizes the amplitude of perturbations and the evolution stage of structures, τ, as measured by the surface density of walls, and $\boldsymbol{q}_1$ and $\boldsymbol{q}_2$ are Lagrangian coordinates of wall boundaries. This relation was corrected for the merging of

neighbouring walls, and this process is described by the erf function in (3.1).

These expressions connect $\tau_{\rm m}$ with the mean surface density of walls and allow us to estimate $\tau_{\rm m}$ from measurements of $\langle q_{\rm w}\rangle$. For other models and/or other distributions of initial perturbations the PDFs similar to (3.1) could be obtained using the technique described in DD99.

3.2.2 *The wall separation*

We have not been able to find a simple theoretical description of the wall separation. None the less, taking into account the mainly 1D character of wall formation, we can roughly link the mean measured wall separation, $\langle D_{\rm sep}\rangle$, to the mean surface density of walls, $\langle q_{\rm w}\rangle$.

Indeed, the matter conservation law along the direction of wall compression can be approximately written as follows:

$$\langle m_{\rm w}\rangle \approx f_{\rm w}\langle n_{\rm p}\rangle\langle D_{\rm sep}\rangle, \quad \langle q_{\rm w}\rangle \approx f_{\rm w}\langle D_{\rm sep}\rangle/l_{\rm v},$$

where $f_{\rm w}$ is the matter fraction assigned to walls. It implies that on average a fraction $f_{\rm w}$ of particles situated at the distance $\pm 0.5 D_{\rm sep}$ from the centre of the wall will be collected by the wall. For simulations when the mean wall separation is comparable to the box size, $L_{\rm box}$, we will use the more accurate relation

$$\langle q_{\rm w}\rangle \approx \frac{f_{\rm dq}}{l_{\rm v}}\left\langle \frac{D_{\rm sep}}{1+D_{\rm sep}/L_{\rm box}}\right\rangle. \tag{3.2}$$

The averaging can be performed analytically assuming the exponential distribution function for the wall separation.

The factor $f_{\rm dq}$ defined by equation (3.2) characterizes the matter fraction assigned to walls as it is determined by comparison of independently measured characteristics $\langle q_{\rm w}\rangle$ and $\langle D_{\rm sep}\rangle$. In turn, difference between $f_{\rm dq}$ and $f_{\rm w}$ characterizes the robustness and degree of self-consistency of the model and the measurements. These estimates are only approximations, because the wall formation is actually a three-dimensional (3D) process.

3.2.3 *Velocity of structure elements*

For the pancakes defined in Section 3.1 the one dimensional velocity of walls, $v_{\rm w}$, can be found from relations (2.2) and (2.3) as follows:

$$v_{\rm w} = \frac{1}{|\boldsymbol{q}_1-\boldsymbol{q}_2|}\int_{q_1}^{q_2} \boldsymbol{n}[\boldsymbol{u}-H(z)\boldsymbol{r}]\,{\rm d}q, \tag{3.3}$$

where $\boldsymbol{n}$ is a unit vector normal to the wall. The small-scale clustering and relaxation of compressed matter does not influence the velocities of walls, and so they are the most stable characteristics of the evolutionary stage reached. As was shown in DD99, the mean velocity of walls, $\langle v_{\rm w}\rangle$, is expected to be negligible as compared with its dispersions, $\sigma_{\rm v}$, and the expected PDF of this velocity, $N_{\rm v}$, is Gaussian for Gaussian initial perturbations.

For the standard spectrum (2.5) with the BBKS transfer function, and for $q_{\rm w} < 1$, the velocity dispersion is related to the amplitude of initial perturbations as follows:

$$\sigma_{\rm v} \approx u_0\tau, \quad \tau_{\rm v} = \frac{\sigma_{\rm v}}{u_0}, \tag{3.4}$$

which is similar to (2.16) and also is identical to expectations of the linear theory. Here $\tau_{\rm v}$ denotes the amplitude τ as measured by the dispersion of wall velocity, and u_0 was introduced by (2.15).

3.2.4 *Velocity dispersion of matter compressed within walls*

The variance of velocity of matter accumulated by walls,

$$w_{wz}^2 = \frac{1}{|\boldsymbol{q}_1-\boldsymbol{q}_2|}\int_{q_1}^{q_2}[\boldsymbol{nu}-H(z)\boldsymbol{nr}-v_{\rm w}]^2\,{\rm d}q, \tag{3.5}$$

can be found in the framework of the Zel'dovich theory using the structure functions described in DD99. As is shown in Appendix A, it can be written as

$$w_{wz}^2(q_{\rm w},\tau) \approx u_0^2\left[\frac{q_w^2}{12}+\frac{\tau^2(1+\beta)^2}{3\beta^2}q_{\rm w}\right], \quad q_{\rm w} \ll 1, \tag{3.6}$$

where β, u_0, $q_{\rm w}$ and $v_{\rm w}$ were introduced by (2.3), (2.4), (2.15), (3.1) and (3.3). In fact, this function characterizes the mean kinetic energy of particles compressed into a wall of a given size $q_{\rm w}$. After averaging over a sample of walls with the PDF $N_{\rm m}$ (3.1), in the Zel'dovich theory, we obtain

$$w_z^2(\tau) = \langle w_{wz}^2(q_{\rm w},\tau)\rangle \approx u_0^2\tau^4\left[7.4+\frac{2.2(1+\beta)^2}{\beta^2}\right]. \tag{3.7}$$

The comparison of the expected mean kinetic energy of the compressed particles with the kinetic energy measured in simulations characterizes the mean degree of relaxation of compressed matter at a given τ.

For richer walls with $q_{\rm w} \gg \langle q_{\rm w}\rangle$, the relation (3.6) is transformed into

$$w_{wz} \approx \frac{u_0}{\sqrt{12}}q_{\rm w}, \tag{3.8}$$

and for such walls, the PDF is similar to (3.1). For a rich sample of walls, this relation can be also used for the direct measurement of the amplitude τ (DMRT; DD99).

3.2.5 *Wall thickness*

The methods discussed in DD99 allow us also, in the framework of the Zel'dovich theory, to obtain the expected thickness of walls along the direction of maximal compression, $h_{\rm w}$. It can be characterized by the thickness of a homogeneous slice with the same surface density. The corresponding expression (Appendix A) is

$$h_{wz}(q_{\rm w},\tau) \approx 2l_{\rm v}\tau\sqrt{q_{\rm w}}(1+z)^{-1}. \tag{3.9}$$

This relation shows that the wall thickness is strongly correlated with its surface density. After averaging with the PDF (3.1), we obtain for the mean thickness of walls

$$\langle h_{wz}\rangle \approx 8\pi^{-1/2}l_{\rm v}\tau^2(1+z)^{-1}. \tag{3.10}$$

The degree of matter compression in the Zel'dovich theory, $\delta_z(q,\tau)$, is characterized by the ratio

$$\delta_z = \frac{q_{\rm w}l_{\rm v}}{h_{\rm w}} = \frac{\sqrt{q_{\rm w}}}{2\tau}.$$

After averaging with the PDF (3.1) we have for the mean degree of matter compression

$$\langle\delta_z\rangle \approx \frac{\langle\sqrt{q_{\rm w}}\rangle}{2\tau} = \frac{2}{\sqrt{\pi}} = 1.13. \tag{3.11}$$

So, in the Zel'dovich theory the averaged degree of matter compression is small.

3.3 Wall properties in redshift space

In observed catalogues only the redshift position of galaxies along the line of sight is known, and therefore the parameters of observed structures with respect to those found above can differ due to the influence of the velocity field. The statistical characteristics of walls in redshift space predicted by the Zel'dovich theory can be found with the methods described above. This information is not so rich as in real space because in redshift space, positions of particles are determined by their velocities, and, for example, such a useful characteristic as the wall velocity cannot be found.

3.3.1 Surface density of walls

In real space (Section 3.1) the pancake formation was defined as an intersection of particles with coordinates $\boldsymbol{q}_1$ and $\boldsymbol{q}_2$. In redshift space the velocity (2.3) along the line of sight must be used instead of the coordinate. In Zel'dovich theory the velocity dispersion exceeds the dispersion of displacement by a factor of $(1+\beta)$. Hence this substitution increases the wall surface density in redshift space with respect to that in real space, and now we must use

$$\tau_{\rm rd} = f_{\rm rd}\tau = \tau\sqrt{(1+\beta)^2\cos\phi^2 + \sin\phi^2}, \tag{3.12}$$

instead of τ. Here the factor $f_{\rm rd} \geq 1$ describes the more effective matter compression in redshift space predicted by the Zel'dovich theory, β was introduced in (2.3), (2.4), and ϕ is a random angle between the direction of wall compression and the line of sight ($0 \leq \phi \leq \pi/2$). Evidently, $\tau_{\rm rd} = \tau$ for $\beta = 0$, so $f_{\rm rd}(\beta = 0) = 1$.

The PDF of wall surface densities in redshift space is identical to (3.1) with a substitution of $\tau_{\rm rd}$ for τ, and now for the mean surface density of walls we have

$$\langle q_{\rm w}\rangle = 8(0.5 + 1/\pi)\langle f_{rd}^2\rangle\tau^2 \approx 6.55\langle f_{rd}^2\rangle\tau^2, \tag{3.13}$$

$$1 \leq \langle f_{rd}^2\rangle = \tfrac{1}{3}[2 + (\beta+1)^2] \leq 2,$$

where τ characterizes the evolutionary stage as before. These relations can probably be used for the description of poorer pancakes and earlier evolutionary stages when the influence of other factors is less important.

At small redshifts we must take into account the influence of the high velocity dispersion of compressed matter generated by the small-scale matter clustering and relaxation. The influence of this factor, well known as the 'finger of God' effect, is opposite to that discussed above. It changes the observed particle position within walls along the line of sight, which blurs the wall boundary and increases the thickness of observed walls. It artificially removes the high-velocity particles from the selected wall, and effectively decreases the surface density of walls selected in redshift space with respect to the estimates (3.13).

The impact of this factor can be approximately described by a modification of PDF of wall surface density,

$$N_m^{rd} = \frac{1}{\sqrt{2\pi}f_{\rm rd}\tau}\frac{1}{\sqrt{q_{\rm w}}}\,{\rm erf}\left(\sqrt{\frac{q_{\rm w}}{8f_{rd}^2\tau^2}}\right) \times\left[\exp\left(-\frac{q_{\rm w}}{8f_{rd}^2\tau^2}\right) - \exp\left(-\frac{q_{\rm w}}{8\tau^2}\right)\times W(q_{\rm w},\tau,\delta_{\rm thr})\right], \tag{3.14}$$

and a new normalization of distribution N_m^{rd}.

The second term in the square brackets describes the artificial rejection of high-velocity particles from the wall with a surface density $q_{\rm w}$ bounded by a threshold density $\delta_{\rm thr}$. In this term the exponent gives the fraction of matter accumulated by the wall in real space for some $q_{\rm w}$ and τ, whereas $W(q_{\rm w}, \tau, \delta_{\rm thr})$ is the fraction of high-velocity particles which are removed from the wall in redshift space. The function $W(q_{\rm w}, \tau, \delta_{\rm thr})$ cannot be found in the Zel'dovich theory, as it depends on the distributions of particles positions and velocities arising due to the small-scale clustering and relaxation of matter compressed within walls.

Another factor which can suppress the expected difference of wall characteristics, measured in real and redshift spaces at small redshifts, is the strong matter condensation within structure elements with various richnesses. The strong matter rearrangement transforms the continuous matter infall on walls into a discontinuous one, increases the separation of infalling structure elements, even in redshift space, and so, at least partly, prevents the erosion of wall boundaries.

These comments show that in redshift space the Zel'dovich theory with the factor $f_{\rm rd}$ given by (3.12) and (3.13) overestimates the matter concentration within walls. Therefore, instead of the factor $f_{\rm rd}$ in (3.13) a factor $\kappa_{\rm rd}(\Gamma,\tau,l_{\rm thr})$ should be used, and the more realistic relation

$$\tau_{\rm m} \approx \sqrt{\frac{q_{\rm w}}{6.55\kappa_{rd}^2}}, \quad 1 \leq \kappa_{\rm rd} \leq f_{\rm rd}, \tag{3.15}$$

connects the amplitude $\tau_{\rm m}$ with the wall richness $q_{\rm w}$ in redshift space.

The actual value of $\kappa_{\rm rd}$ depends on the parameters of the cosmological model and on the method of identification of walls. The analysis performed below shows that for the walls selected in 3D space as described in Section 6.1, no growth of $q_{\rm w}$ was found, and the parameters $q_{\rm w}$ and $\tau_{\rm m}$ are connected by the relation (3.1) as in real space.

3.3.2 Wall separation

The separations of richer walls is not sensitive to relatively small shifts of particle positions introduced by the random velocities, but these shifts can result in an artificial merging of poorer walls. The influence of this factor can be tested with the relation (3.2) as before.

3.3.3 Velocity dispersion of matter compressed within walls and the wall thickness

In redshift space the expression for the velocity dispersion of matter compressed within walls in the Zel'dovich theory is identical to (3.6) with a substitution of $\tau_{\rm rd} = \tau\kappa_{\rm rd}$ instead of τ, but now it characterizes also the observed thickness of walls. For walls selected from the 3D sample of particles, as described in Section 6.1, we have

$$h_{\rm w} = \sqrt{12}w_{\rm w}H_0^{-1}, \tag{3.16}$$

$$w_{\rm w} = u_0\sqrt{\frac{q_w^2\beta^2}{12} + \frac{\tau^2\kappa_{rd}^2 q_{\rm w}}{3}(1+\beta)^2}. \tag{3.17}$$

This value exceeds the corresponding real thickness of walls given by (3.9). The expected overdensity of compressed matter is given by

$$\delta_{\rm rd} = l_{\rm v}\langle q_{\rm w}/h_{\rm w}\rangle. \tag{3.18}$$

4 MEASURED CHARACTERISTICS OF LARGE-SCALE MATTER DISTRIBUTION

4.1 Core-sampling approach

The core-sampling approach was proposed by Buryak, Doroshkevich & Fong (1994) for the analysis of the galaxy distribution in deep pencil-beam redshift surveys. In the original form it allows us to obtain the mean free-path between the filaments and walls. It was improved and described in detail in LCRS1, where some characteristics of the large-scale galaxy distribution were found for the Las Campanas Redshift Survey. For simulated matter distributions as considered here these characteristics were discussed in DMRT.

The potential of the core-sampling approach is not exhausted by these applications, and it could be used to measure parameters of the large-scale matter distribution discussed in the previous sections. Here we will use this approach to obtain the characteristics of the wall-like structure component.

The core-sampling method deals with a sample of points (galaxies) lying within relatively narrow cores–rectangular and/or cylindrical in simulations, and conical in observations–and it studies the point distribution along these cores. For some applications the transversal coordinates of points can be used as well. To take into account the selection effects, which are important for observed catalogues, appropriate corrections can be incorporated. The sampling core is characterized by the size, $D_{\rm core}$, that is the side of a rectangular core or the angular diameter of a conical core.

4.2 Measured characteristics of walls

Here we will apply the core-sampling technique to the sample of wall-like structure elements selected by a 3D cluster analysis (DMRT; see Section 6.1). This means that the sampling cores contain only the particles assigned to walls. Further on, all particles are projected on to the core axes and are collected into a set of clusters with a linking length $l_{\rm link}$. Clusters with richness larger than a threshold richness, $N_{\rm min}$, are identified with walls within the sampling core.

The measured wall parameters are sensitive to the influence of small-scale clustering of matter within walls. For strongly disrupted walls and a narrow core, the results depend on the random position of high-density clumps, which strongly increases the scatter of measured wall properties. The influence of this factor is partly suppressed for larger sizes of the sampling core, $D_{\rm core}$.

However, the random intersection of the core with a wall boundary generates artificially poor clusters. The number of such intersections increases proportionally to $D_{\rm core}$, which restricts the maximal $D_{\rm core}$. To suppress the influence of this factor, a threshold richness of cluster, $N_{\rm min}$, was used. If, however, $N_{\rm min}$ becomes too large, the statistical estimates become unreliable. For large $D_{\rm core}$ the overlapping of projections of neighbouring walls also becomes important which distorts the measured wall characteristics.

It is also important to choose an optimal linking length, $l_{\rm link}$, because for small $l_{\rm link}$, only the high-density part of walls is measured, whereas for larger $l_{\rm link}$, again the impact of the random overlapping of wall projections becomes important.

The influence of these factors cannot be eliminated completely, and our final estimates of properties of walls are always distorted to some degree. These distortions can be minimized for an optimal range of parameters $D_{\rm core}$, $N_{\rm min}$ and $l_{\rm link}$. Practically, these factors do not distort the velocity dispersion of walls, $\sigma_{\rm v}$, which therefore provides the best characteristic of the actual evolutionary stage of the wall formation. On the other hand, the comparison of results obtained for different $l_{\rm link}$ and $D_{\rm core}$ allows us to characterize the inner structure of walls.

4.2.1 *Measurement and correction of wall parameters*

The richness of clusters in the core measures the surface density of walls,

$$m_{\rm sim} = \frac{N_{\rm m}}{D_{core}^2}, \tag{4.1}$$

where $N_{\rm m}$ is the number of particles in a cluster. The velocity of walls, $v_{\rm sim}$, the velocity dispersion of particles accumulated within walls, $w_{\rm sim}$, and the proper sizes of walls, $h_{\rm sim}$, are found as follows:

$$r_{\rm w} = \frac{1}{N_{\rm m}}\sum_{i=1}^{N_{\rm m}} r_i, \quad v_{\rm sim} = \frac{1}{N_{\rm m}}\sum_{i=1}^{N_{\rm m}}(u_i - Hr_i),$$

$$w_{sim}^2 = \frac{1}{N_{\rm m}-1}\sum_{i=1}^{N_{\rm m}}(u_i - Hr_i - v_{\rm sim})^2, \tag{4.2}$$

$$h_{sim}^2 = \frac{12}{N_{\rm m}-1}\sum_{i=1}^{N_{\rm m}}(r_i - r_{\rm w})^2.$$

Here r_i, $r_{\rm w}$ and u_i are the coordinates of a particle, of a wall, and the velocity of a particle along the sampling core, respectively. The wall separation, $D_{\rm sim}$, is measured by the distance between neighbouring clusters.

The parameters $m_{\rm sim}$, $v_{\rm sim}$, $w_{\rm sim}$ and $h_{\rm sim}$ as given by (4.1) and (4.2) are found along the sampling core, and so are not identical to the parameters discussed in Section 3. These parameters must be corrected for the random orientation of walls with respect to the sampling core. The impact of this factor increases the measured surface density, and the corrected wall surface density, $m_{\rm c}$, is connected with the measured one by

$$m_{\rm c} = m_{\rm sim}\cos\phi, \quad 0 \le \phi \le \pi/2,$$

$$\langle m_{\rm c}\rangle = 0.5\langle m_{\rm sim}\rangle, \tag{4.3}$$

where ϕ is a random polar angle between the core and the vector orthogonal to the surface of the wall, and the averaging is performed in a spherical coordinate system. Corrected values of the wall velocity and the walls thickness are as follows:

$$v_{\rm c} = v_{\rm sim}\sqrt{3}, \quad h_{\rm c} = h_{\rm sim}/\sqrt{3}. \tag{4.4}$$

In redshift space the wall thickness is connected with the velocity dispersion by (3.16). The velocity dispersion within walls was found to be almost isotropic (DMRT), and so we will use the measured $w_{\rm sim}$ as the actual velocity dispersion across walls.

The measured PDF of the wall surface density, $N_{\rm m}(m_{\rm c})$, and the mean wall surface density, $\langle m_{\rm c}\rangle$, are distorted due to the small-number statistics of rich walls and rejection of poor walls with a richness $N_{\rm m} \le N_{\rm min}$. The correction for these distortions can be estimated by comparing the simulated PDF with the expected PDF (3.1).

To do this, we will fit the measured PDF to the function

$$N_{\rm m} = \frac{a_{\rm m}}{\sqrt{x_{\rm m}}}{\rm e}^{-x_{\rm m}}{\rm erf}(\sqrt{x_{\rm m}}), \quad x_{\rm m} = \frac{b_{\rm m}m_{\rm sim}}{\langle m_{\rm sim}\rangle}. \tag{4.5}$$

Table 1. Parameters of simulated DM and mock catalogues.

sample	$\Omega_{\rm m}$	h	τ_T	σ_8	r_0 h^{-1} Mpc	γ	τ_ξ	$\sigma_{\rm vel}/\sqrt{3}$ km s^{-1}	$\tau_{\rm vel}$
SCDM	1	0.5	0.68	1.37	6.5	1.9	0.94	670	0.51
ΛCDM	0.35	0.7	0.37	1.11	6.0	1.8	0.34	554	0.37
OCDM	0.5	0.6	0.29	0.74	5.0	1.3	0.25	346	0.23
$mock_1$	0.5	0.6	0.29	0.95	6.0	1.4	0.28	370	0.25
$mock_2$	0.5	0.6	0.29	0.95	6.0	1.4	0.28	370	0.24
$mock_3$	0.5	0.6	0.29	1.24	7.0	1.5	0.33	374	0.24
$mock_4$	0.5	0.6	0.29	1.61	8.0	1.6	0.39	404	0.26

r_0 and γ are the correlation lengths and the slope of correlation function (2.11) in redshift space; σ_8, τ_T and τ_ξ are the amplitudes of perturbations as given by (2.9) and (2.12), $\sigma_{\rm vel}$ and $\tau_{\rm vel}$ are the velocity dispersion of all particles and amplitudes of perturbations measured by $\sigma_{\rm vel}$ as given by (2.16).

The parameter $b_{\rm m}$ describes deviations of measured and expected mean surface density of walls $\langle m_{\rm sim}\rangle$, and $a_{\rm m}$ is a normalization factor. If the measured PDF is well fitted to the function (4.5), then the value

$$m_{\rm t} = \langle m_{\rm c}\rangle / b_{\rm m} \tag{4.6}$$

can be taken as a measure of the 'true' mean surface density of walls.

Finally, the mean dimensionless surface density of walls, $\langle q_{\rm w}\rangle$, and the amplitudes of perturbations, $\tau_{\rm m}$ and $\tau_{\rm v}$, measured by the surface density and velocity of wall-like structure elements, can be estimated as follows:

$$\langle q_{\rm w}\rangle = \frac{\langle m_{\rm sim}\rangle}{2 b_{\rm m} l_{\rm v} \langle n_{\rm p}\rangle}, \quad \tau_{\rm m} = \sqrt{\frac{\langle q_{\rm w}\rangle}{6.55}}, \quad \tau_{\rm v} = \frac{\sqrt{\langle v_{sim}^2\rangle}}{u_0}. \tag{4.7}$$

The small-number statistics of rich and poor walls distorts also the measured wall separation, $D_{\rm sep}$. The expected distribution of wall separations is exponential, and therefore it is possible to correct the mean separation using the fit of the measured PDF, $N_{\rm sep}(D_{\rm sim})$, to the function

$$N_{\rm sep} = a_{\rm sep} \exp(-b_{\rm sep} D_{\rm sim} / \langle D_{\rm sim}\rangle). \tag{4.8}$$

As before, the parameter $b_{\rm sep}$ describes deviations of the measured and expected mean separation of walls, and $a_{\rm sep}$ is a normalization factor. If the measured PDF is well fitted to the function (4.8), then the value

$$\langle D_{\rm sep}\rangle = \langle D_{\rm sim}\rangle / b_{\rm sep}, \tag{4.9}$$

can be taken as a measure of the 'true' mean separation of walls.

5 GENERAL CHARACTERISTICS OF THE SIMULATED MATTER DISTRIBUTION

5.1 Basic simulations

The theoretical model discussed above describes the evolution of the DM distribution and so should be tested with the simulated DM distribution as well. Here we use three simulations as a basis for our analysis–the *COBE*-normalized standard CDM model (SCDM), a ΛCDM with $\Omega_\Lambda > \Omega_{\rm m}$, and an open CDM (OCDM) model. These models were described and investigated with 3D cluster analysis and Minimal Spanning Tree technique in DMRT. It was found that the ΛCDM and OCDM models successfully reproduce the main observed characteristics of large-scale matter distribution, while the SCDM model demonstrates strong signatures of over-evolution. Here we study these three models, bearing in mind that only the ΛCDM and OCDM models can be considered as realistic models of the observed large-scale matter distribution. The SCDM model represents the matter distribution typical for a late evolutionary stage.

The simulations were performed with a PM code in a box of $(500\,h^{-1}\,{\rm Mpc})^3$ with $(300)^3$ particles for the Harrison–Zel'dovich primordial power spectrum and the BBKS transfer function. The force and mass resolutions are $\sim 0.9\,h^{-1}\,{\rm Mpc}$ and $\sim 10^{11}\,{\rm M}_\odot$, respectively. The point distribution in redshift space was produced by adding an apparent shift to one coordinate due to the peculiar velocity of particles.

Four mock catalogues were prepared on the basis of the OCDM model with various degrees of large-scale bias between the spatial DM distribution and the 'galaxies'. These mock catalogues were constructed by identifying randomly 'galaxies' with DM particles, but with a probability depending on the environmental density, thereby identifying more particles as 'galaxies' in high-density regions (walls). These catalogues were investigated also in both real and redshift spaces.

The main characteristics of the simulations are listed in Table 1. A more detailed description can be found in DMRT.

5.2 Large-scale amplitude of perturbations

The evolutionary stages reached in the models under discussion can be suitably characterized using the methods described in Section 2. The value τ_T listed in Table 1 characterizes the large-scale amplitude used for the normalization of simulated perturbations. Other measures of the amplitude, such as σ_8, τ_ξ and $\tau_{\rm vel}$, are sensitive both to the actually realized sample of random perturbations (cosmic variance) and to the non-linear distortions of power spectrum produced during the evolution. For the considered mock catalogues these measures are also sensitive to the large-scale bias between the spatial DM and 'galaxies' distributions, which allows us to characterize it quantitatively.

The spatial matter distribution and the bias between spatial distributions of DM component and 'galaxies' can be characterized by the correlation length, r_0, and the slope of the correlation function, γ, introduced in (2.11). These parameters are listed in Table 1 for all samples. Using relations (2.12) and (2.13), these values allows us to calculate σ_8 and τ_ξ, which are also listed in Table 1.

The characteristics of correlation function, r_0 and γ, are sensitive to the perturbations in scales $k \sim 0.5$–$0.1\,h\,{\rm Mpc}^{-1}$. As is seen from (2.12), estimates τ_ξ are very sensitive to the value of $2-\gamma$, and so to small-scale perturbations. The first zero-point of

the autocorrelation function, $r_\xi \approx 40\,h^{-1}$ Mpc, can be usually found with a large uncertainty (~20–30 per cent) but its impact is reduced by the small exponent $1 - \gamma/2 \leq 0.3$ in (2.12).

For OCDM and ΛCDM models the impact of small-scale matter clustering is moderate, and differences between $\tau\xi$ and $\tau_{\rm vel}$ are found to be ~10 per cent. The differences between the same parameters and τ_T can be considered as a reasonable measure of simulated 'cosmic variance'. For these models differences between the parameter τ_ξ calculated for real and redshift spaces also do not exceed ~10 per cent. For the SCDM model both τ_ξ and $\tau_{\rm vel}$ are distorted by the strong small-scale clustering. This divergence indicates that for the SCDM model the successful application of methods discussed in Section 3 is also in question.

The progressive growth of τ_ξ and σ_8 for mock catalogues characterizes the degree of the large-scale bias between the spatial distribution of DM component and 'galaxies'.

6 PROPERTIES OF WALL-LIKE STRUCTURE ELEMENTS

The main basic characteristics of walls were discussed in DMRT for three DM and four mock catalogues mentioned above both in real and redshift spaces. In this section the wall characteristics discussed in Section 3 are found with the core-sampling technique for the same simulations and the same samples of walls.

6.1 Selection of wall-like structure elements

The sample of wall-like structure elements was selected by the two-parameter method described and exploited in DMRT. It identifies the wall-like structure elements with clusters found using a threshold linking length, $l_{\rm thr}$, and a threshold richness, $N_{\rm thr}$. As usual, the boundary of the clusters is defined by the threshold overdensity, $\delta_{\rm thr}$, which is connected with the threshold linking length by

$$\delta_{\rm thr} = \frac{n_{\rm thr}}{\langle n\rangle} = \frac{3}{4\pi\langle n\rangle l_{thr}^3}. \qquad (6.1)$$

The threshold richness, $N_{\rm thr}$, restricts the matter fraction, $f_{\rm w}$, associated with walls.

The main characteristics of these samples both in real and redshift spaces are listed in Table 2. The values of $f_{\rm w} \approx 0.4$–0.45 are consistent with the theoretically expected and observed matter fraction accumulated by walls (DD99; LCRS1; LCRS2). The analysis performed in DMRT shows that for the low-density models the main characteristics of such wall-like elements are similar to the observed characteristics of superclusters of galaxies (Oort 1983, 1984; LCRS2; DURS).

6.2 DM walls in real space

The analysis of DM catalogues in real space is most interesting, as in this case we can study the clear signal from the gravitational interaction of compressed matter, and can reveal and characterize statistically the matter relaxation. Five basic characteristics of DM walls discussed in Section 3, namely, the wall thickness, $h_{\rm w}$, the dispersions of wall velocities, $\sigma_{\rm v}$, the velocity dispersion of matter compressed within walls, $w_{\rm w}$, the dimensionless surface density, $q_{\rm w}$, and mean separation of walls, $D_{\rm sep}$, can be found with the core-sampling method, and can be compared with those found in DMRT. The surface density of walls is closely connected with the size of protowalls, as discussed in DMRT.

Comparison of such characteristics of matter distribution as $\tau_{\rm vel}$ listed in Table 1 and $\tau_{\rm v}$ and $\tau_{\rm m}$ related to the wall properties allows us to test the influence of small-scale matter clustering and other random factors discussed in Section 4.3, and to find the optimal ranges of core size, $D_{\rm core}$, and of threshold richness, $N_{\rm min}$, as well as the optimal linking length, $l_{\rm link}$. The results listed in Table 2 are obtained with the linking length $l_{\rm link} = 5\,h^{-1}$ Mpc, and are averaged over seven core sizes, $6\,h^{-1}$ Mpc $\leq D_{\rm core} \leq 9\,h^{-1}$ Mpc, and over seven threshold richnesses, $10 \leq N_{\rm min} \leq 35$.

6.2.1 *Basic characteristics of DM walls*

For all models, the dispersion of wall velocities, $\sigma_{\rm v}$, is found to be

Table 2. Wall characteristics in real and redshift spaces.

sample	$\delta_{\rm thr}$	$f_{\rm w}$	$f_{\rm cr}$	$\langle q_{\rm w}\rangle$	$\langle\tau_{\rm m}\rangle$	$\langle\tau_{\rm v}\rangle$	$\langle\delta\rangle$	$\langle h_{\rm w}\rangle$ h^{-1}Mpc	$\langle w_{\rm w}\rangle$ km s^{-1}	$\langle\epsilon\rangle$	$p_{\rm w}$	$\langle D_{\rm sep}\rangle$ h^{-1}Mpc	$f_{\rm dq}$
real space													
SCDM	2.5	0.44	0.74	1.00 ± 0.18	0.39 ± 0.04	0.58	4.7	3.4 ± 0.4	463 ± 18	0.1	0.27	43 ± 8	0.4
ΛCDM	1.6	0.46	0.85	0.83 ± 0.16	0.35 ± 0.03	0.39	7.4	4.0 ± 0.3	387 ± 20	0.2	0.30	71 ± 13	0.4
OCDM	1.3	0.40	0.88	0.52 ± 0.06	0.28 ± 0.02	0.26	2.4	6.0 ± 0.7	330 ± 33	0.8	0.44	46 ± 8	0.3
mock$_1$	1.6	0.43	0.82	0.87 ± 0.15	0.36 ± 0.03	0.27	5.0	7.0 ± 1.1	412 ± 51	0.9	0.48	84 ± 17	0.3
mock$_2$	1.3	0.44	0.81	0.84 ± 0.13	0.36 ± 0.03	0.27	5.1	6.6 ± 0.9	394 ± 45	0.8	0.47	78 ± 13	0.3
mock$_3$	1.3	0.45	0.84	0.88 ± 0.11	0.36 ± 0.02	0.27	5.6	5.2 ± 0.6	354 ± 27	0.6	0.43	73 ± 11	0.4
mock$_4$	1.3	0.44	0.86	1.23 ± 0.17	0.43 ± 0.03	0.28	9.1	4.5 ± 0.4	359 ± 20	0.5	0.39	78 ± 14	0.5
mock$_4$	1.3	0.48	0.87	1.35 ± 0.19	0.45 ± 0.03	0.27	7.5	5.6 ± 0.5	379 ± 26	0.7	0.40	81 ± 12	0.5
redshift space													
SCDM	2.5	0.41	0.88	0.84 ± 0.08	0.36 ± 0.02	–	1.8	8.5 ± 0.8	245 ± 23	–	0.75	45 ± 9	0.3
ΛCDM	2.1	0.45	0.88	0.76 ± 0.13	0.34 ± 0.03	–	2.6	7.2 ± 0.6	207 ± 17	–	0.48	63 ± 11	0.4
OCDM	1.3	0.44	0.77	0.56 ± 0.10	0.29 ± 0.03	–	1.4	11.2 ± 1.3	323 ± 36	–	0.58	49 ± 8	0.3
mock$_1$	1.2	0.43	0.82	0.89 ± 0.16	0.37 ± 0.03	–	2.7	13.3 ± 2.3	385 ± 66	–	0.71	87 ± 18	0.3
mock$_2$	1.5	0.43	0.83	0.86 ± 0.13	0.36 ± 0.03	–	2.7	12.2 ± 1.9	353 ± 54	–	0.70	86 ± 25	0.3
mock$_3$	1.8	0.44	0.86	0.85 ± 0.09	0.36 ± 0.02	–	2.9	9.5 ± 1.1	276 ± 32	–	0.70	83 ± 17	0.3
mock$_4$	1.8	0.45	0.84	1.10 ± 0.13	0.41 ± 0.02	–	4.1	8.8 ± 0.9	254 ± 25	–	0.65	87 ± 21	0.4
mock$_4$	1.3	0.46	0.82	1.22 ± 0.13	0.43 ± 0.02	–	3.8	10.1 ± 0.9	291 ± 26	–	0.61	89 ± 16	0.4

Here $\delta_{\rm thr}$ is threshold parameters of clusters, $f_{\rm w}$ is the fractions of all particles forming the selected walls, and $f_{\rm cr}$ is the fraction of particles belonging to walls in both real and redshift spaces. Parameters $\tau_{\rm m}$,$\tau_{\rm v}$ are the amplitude of perturbations as given by (3.1) and (3.4). The other quantities are explained in the text. Averaging was performed over seven core sizes, $6\,h^{-1}$ Mpc $\leq D_{\rm core} \leq 9\,h^{-1}$ Mpc, and over seven threshold richnesses, $10 \leq N_{\rm min} \leq 35$ for the linking length $l_{\rm link} = 5\,h^{-1}$ Mpc.

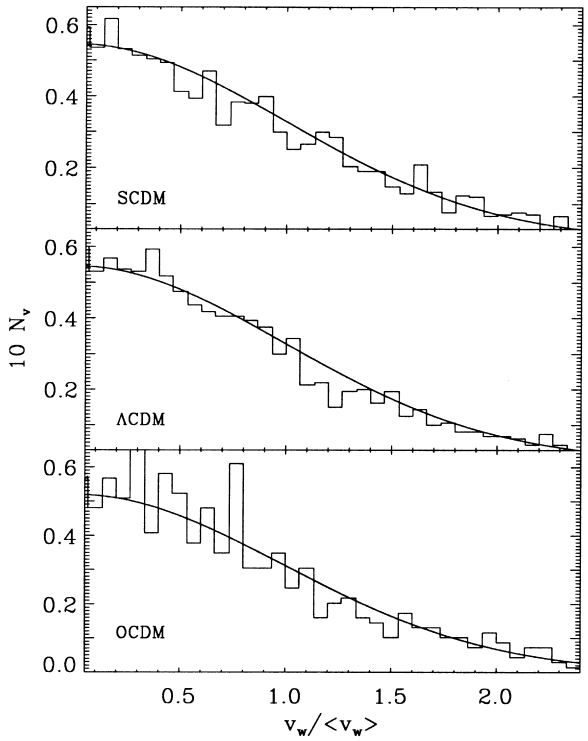

Figure 1. PDFs of DM wall velocity, $N_{\rm v}(v_{\rm w}/\langle v_{\rm w}\rangle)$, in real space for SCDM, ΛCDM and OCDM models. The Gaussian fits are shown by solid lines.

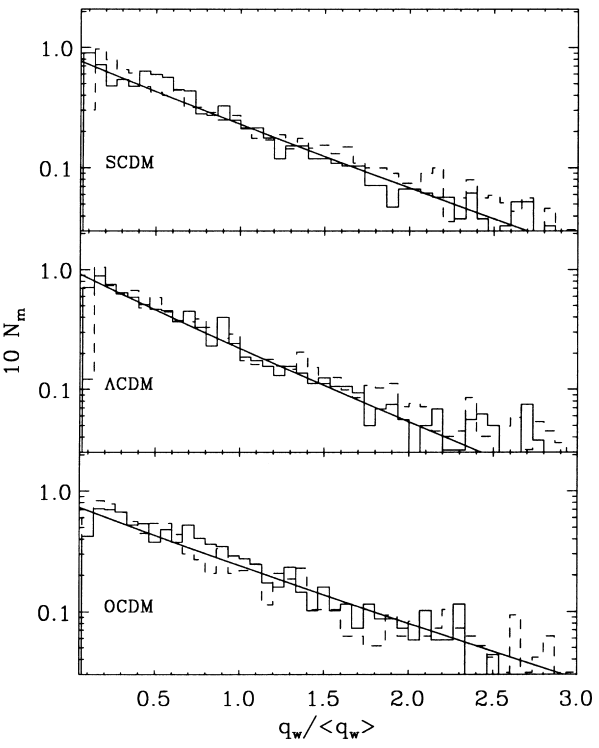

Figure 2. PDFs of the DM wall surface density, $N_{\rm m}(q_{\rm w}/\langle q_{\rm w}\rangle)$, in real (solid lines) and redshift (dashed lines) spaces for SCDM, ΛCDM and OCDM models. The fits (3.1) are shown by solid lines.

the best and most stable characteristic of the evolutionary stage reached. This is the direct consequence of the discrimination between the wall velocity and the velocity dispersion of particles compressed within walls. The PDFs, $N_{\rm v}$, plotted in Fig. 1, are well fitted to Gaussian functions with the measured dispersion.

For the OCDM and ΛCDM models the mean dimensionless surface density of walls, $\langle q_{\rm w}\rangle$, and the amplitudes, $\tau_{\rm m} \approx \tau_{\rm v} \approx \tau_{\rm vel}$, are found with scatters ∼10–15 per cent for the adopted $N_{\rm min}$, $D_{\rm core}$ and $l_{\rm link}$. This scatter characterizes the moderate action of random factors discussed in Section 3.2, and the procedure of measurement. The values of $l_{\rm v}\langle q_{\rm w}\rangle$ are consistent with estimates of the size of protowalls obtained in DMRT. The PDFs of the surface density plotted in Fig. 2 are consistent with that expected from (3.1). These results demonstrate that for lower density cosmological models the Zel'dovich approximation successfully describes these basic characteristics of rich walls.

For the SCDM model, the results listed in Table 2 are more sensitive to the method of measurement, and the surface density of walls is underestimated, $\tau_{\rm m} < \tau_{\rm v} \approx \tau_{\rm vel}$. This difference can be mainly ascribed to the strong disruption of walls occurring at late evolutionary stages in this model. Other important factors are the faster compression and/or expansion of walls in transversal directions, and the existence of richer haloes of evaporated particles around the walls mixed with infalling particles. Such a halo becomes richer for larger τ, i.e., for the ΛCDM, and especially for the SCDM models.

The distribution function of wall separation, $N_{\rm sep}$, plotted in Fig. 3 is well fitted to (truncated) exponential distribution. The mean wall separation $\langle D_{\rm sep}\rangle$ is sensitive to the threshold richness $N_{\rm min}$ and to the core size $D_{\rm core}$. The separation $\langle D_{\rm sep}\rangle \sim 40\,h^{-1}$ Mpc, found for the lower threshold richness, $N_{\rm min} = 5$, and larger core sizes, $D_{\rm core} = 9\,h^{-1}$ Mpc, coincides with the results obtained in DMRT. It increases with $N_{\rm min}$ as the number of rich walls progressively decreases. For smaller $D_{\rm core}$ and larger $N_{\rm min}$ some of highly disrupted walls are lost due to their small covering factor. This parameter can be found with relatively large scatter.

Using relation (3.2), we can compare our estimates of $\langle D_{\rm sep}\rangle$ and $\langle q_{\rm w}\rangle$. For all models we have

$$f_{\rm dq} \approx (0.75\text{–}0.9) f_{\rm w}, \tag{6.2}$$

and the mean wall separation is probably overestimated.

For all models under consideration, the mean wall thickness, $\langle h_{\rm w}\rangle$, is similar to that found in DMRT with the inertia tensor technique, where a wall is represented by a homogeneous ellipsoid. It is about 2–4 times smaller than that expected in the Zel'dovich approximation (3.10) which is an indication of the relaxation of gravitationally bounded DM particles within walls.

For the OCDM model the velocity dispersion of matter compressed within walls is found to be similar to the mean velocity of walls and of all particles, $\langle w_{\rm w}\rangle \sim \sigma_{\rm v} \approx \sigma_{\rm vel}$. In contrast, for the SCDM and ΛCDM models the dispersion $\langle w_{\rm w}\rangle$ is about 30 per cent smaller than that obtained for the complete walls in DMRT and the dispersions $\sigma_{\rm vel}$ and $\sigma_{\rm v}$ discussed above. This divergence characterizes statistically the evaporation of high-energy particles in the course of the relaxation of compressed matter, and is reinforced by the procedures of measurement and wall selection. The relatively small value of $\langle w_{\rm w}\rangle$ demonstrates that, in contrast to the clusters of galaxies, the moderate degree of 1D matter compression within walls is not accompanied by a significant increase of velocity dispersion.

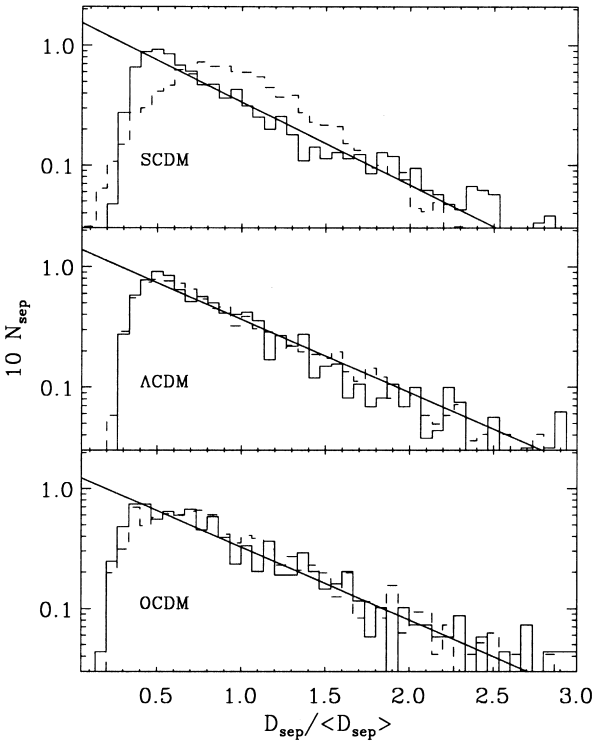

Figure 3. PDFs of DM wall separations, $N_{\rm sep}(D_{\rm sep}/\langle D_{\rm sep}\rangle)$, in real (solid lines) and redshift (dashed lines) spaces for SCDM, ΛCDM and OCDM models. The exponential fits are shown by solid lines.

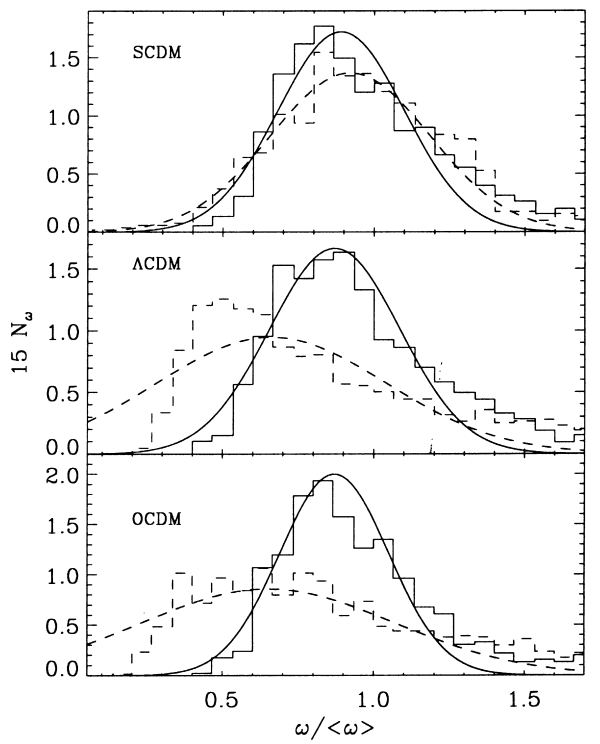

Figure 4. PDFs of the reduced velocity dispersion, $N_\omega(\omega/\langle\omega\rangle)$, for DM walls in real (solid lines) and redshift (dashed lines) spaces for SCDM, ΛCDM and OCDM models. The Gaussian fits are also shown by solid and dashed lines.

6.2.2 *Relaxation of compressed matter*

For ΛCDM and SCDM models the wall thickness, $h_{\rm w} \sim (3\text{–}4)\,h^{-1}\,$Mpc, is 2–3 times smaller than that expected in the Zel'dovich theory (3.10). So, large compression of matter within walls means that the selected particles are strongly confined and, probably, relaxed. For 1D matter compression the relaxation is expected to be weak, but in reality it is reinforced due to the small-scale clustering and disruption of walls.

The degree of relaxation reached can be characterized by the parameters $\langle\delta\rangle$ and $\langle\epsilon\rangle$,

$$\langle\delta\rangle = \left\langle \frac{l_{\rm v} q_{\rm w}}{h_{\rm w}} \right\rangle, \quad \langle\epsilon\rangle = \frac{\langle w_w^2\rangle}{w_z^2(\tau)}, \tag{6.3}$$

listed in Table 2. Here $\langle\delta\rangle$ measures the mean degree of matter compression, and $\langle\epsilon\rangle$ is the mean kinetic energy of compressed particles with respect to the expectations of the Zel'dovich theory. The function $w_{\rm z}(\tau)$ given by (3.7) is evaluated at $\tau = \tau_{\rm v}$.

The divergence between the expectations of the Zel'dovich theory and simulations is moderate for the OCDM model, and becomes strong for the ΛCDM model as the evolution progresses. For the SCDM model the estimate of $\langle\delta\rangle$ is artificially decreased, together with $\langle q_{\rm w}\rangle$. The small value of $\langle\epsilon\rangle \sim 0.1\text{–}0.2$ confirms an essential deficit of energy of compressed particles in comparison to that expected in the Zel'dovich theory. This deficit is partly enhanced by the procedure of wall selection, as the wall boundaries are blurred, and particles placed far from the wall centre are not included into walls.

In the Zel'dovich theory the strong correlation of $w_{\rm w}$ and $h_{\rm w}$ with the wall richness, $m_{\rm w}$, is described by expressions (3.6) and (3.9). In simulations the measured linear correlation coefficients of $q_{\rm w}$, $w_{\rm w}$ and $h_{\rm w}$ are also ~0.4–0.5, which indicates that the essential mass dependence of these parameters remains also after relaxation. To discriminate the regular and random variations of functions $w_{\rm w}$ and $h_{\rm w}$, we will consider the *reduced* wall thickness, ζ, and the *reduced* velocity dispersion, ω, which can be defined as follows:

$$h_{\rm w} = \langle h_{\rm w}\rangle \mu^{p_h} \zeta, \quad w_{\rm w} = \langle w_{\rm w}\rangle \mu^{p_{\rm w}} \omega, \tag{6.4}$$

$$\mu = m_{\rm w}/\langle m_{\rm w}\rangle = q_{\rm w}/\langle q_{\rm w}\rangle, \quad p_h \approx p_{\rm w} \approx 0.3\text{–}0.4,$$

$$\langle\zeta\rangle \approx \langle\omega\rangle \approx 1, \quad \sigma_\zeta \approx \sigma_\omega \approx 0.2.$$

In all considered cases the PDFs of the reduced velocity dispersion within walls, N_ω, and of the reduced wall thickness, N_ζ, can be roughly fitted to Gaussian functions. The PDFs N_ω are plotted in Fig. 4 for all three models.

These results show that due to the strong relaxation of compressed matter the correlations between the considered characteristics of walls predicted by the Zel'dovich theory in equations (3.6), (3.8) and (3.10) are replaced by relations (6.4), which are also universal.

6.3 DM walls in redshift space

If the analysis of wall characteristics in real space allows us to reveal the influence of gravitational interaction of the compressed matter, then a similar analysis performed in redshift space reveals the influence of random velocities on the observed characteristics of the large-scale matter distribution.

In redshift space the analysis of wall characteristics was performed for samples of walls selected as described in Section

6.1. As was shown in DMRT, in low-density cosmological models the main characteristics of these walls are similar to the observed characteristics of superclusters of galaxies. The determination of wall characteristics and their corrections are discussed in Section 4.3. The wall parameters were found in the same ranges of $D_{\rm core}$ and $N_{\rm min}$ as in real space for $l_{\rm link} = 5\,h^{-1}$ Mpc.

The main results are listed in Table 2, and are plotted in Figs 2–4.

6.3.1 *Walls in real and redshift spaces*

The samples of walls selected in real and redshift spaces are not identical with each other due to influence of random velocities of particles. This difference can be suitably characterized by the fraction of the same particles assigned to walls in both spaces. Here this fraction was defined as a ratio of number of the particles, N_{com}, to the number of particles assigned to the selected walls, $N_{\rm w}$. For all models under consideration this fraction, listed in Table 2, is

$$f_{\rm cr} = N_{com}/N_{\rm w} \sim 0.8\text{–}0.9.$$

Small variations of the number of particles, $N_{\rm w}$, assigned to walls in real and redshift spaces lead to these variations.

These results indicate that the influence of high random velocities generated by the small scale wall disruption and the matter relaxation moderately distorts the sample of walls selected in redshift space. More strong deviations between such wall parameters as the wall thickness and degree of matter compression, measured in real and redshift spaces, are caused by the redistribution of matter within walls and the procedure of measurement, rather than by the incorrect wall identification. The impact of these factors rapidly increases with $\tau_{\rm m}$, and becomes extreme for the SCDM model.

These deviations can be sensitive to the code used for simulation (see, e.g., discussion in Splinter et al. 1998). For example, in the P^{3}M code, these variations may increase due to the larger velocities of compressed matter generated there.

6.3.2 *Basic characteristics of DM walls*

For all three models the mean surface density of selected walls listed in Table 2 is similar to that found in real space. This fact shows that the artificial growth of matter concentration within walls discussed in Section 3.2 is effectively suppressed by the influence of the velocity dispersion and the procedure of wall selection, and the relation (3.1), as before, connects the mean surface density of selected walls, $\langle q_{\rm w}\rangle$, with the amplitude, $\tau_{\rm m}$. Variations of $\langle q_{\rm w}\rangle$ and $\tau_{\rm m}$ with $D_{\rm core}$ and $N_{\rm min}$ are shown in Table 2 as a scatter of these parameters. The PDFs $N_{\rm m}$ plotted in Fig. 2 are also similar to those found in real space.

The mean wall separation is consistent with the estimate found in real space and, as before, for all models $f_{\rm dq} \approx (0.75\text{–}0.9) f_{\rm w}$. The PDFs $N_{\rm sep}$ plotted in Fig. 3 are also similar to those found in real space.

In redshift space the adopted method of wall identification selects mainly particles with a small relative velocity, which essentially restricts the measured velocity dispersion within walls and the wall thickness. Results listed in Table 2 show that only for the OCDM model, the velocity dispersion of compressed matter is consistent with the values found in real space and in DMRT. For ΛCDM and SCDM models they are even smaller than those found in real space. The measured wall thickness is now linked with the velocity dispersion by the relation (3.16).

6.3.3 *Characteristics of matter relaxation*

In redshift space walls are less conspicuous than in real space but, even so, for all three models the mean overdensity, $\langle\delta\rangle$, listed in Table 2, differs from the estimates based on the Zel'dovich theory (3.7). As in real space, the velocity dispersion in redshift space is strongly correlated with the surface density of walls, which is described by the relation (6.4) with an exponent $p_{\rm w} \approx 0.5$. The PDFs of the reduced velocity dispersions, N_ω, plotted in Fig. 4, demonstrate some excess of particles with lower ω, but it can also be roughly fitted to a Gaussian function with $\langle\omega\rangle \approx 1$ and dispersion $\sigma_\omega \approx 0.4$. This dispersion is about 2 times larger than that in real space.

These results show that, although in redshift space walls are not so conspicuous as in real space, in the range of 'time' $\sim 0.2 \leq \tau \leq \sim 0.5$, the relaxation of compressed dark matter can be directly recognized by these methods.

6.4 Walls in mock catalogues

The analysis of mock catalogues characterizes how the considered simple model of large-scale bias influences the measured wall properties. These catalogues were investigated also in both real and redshift spaces. The analysis was performed for 10 values $N_{\rm min}$ ($15 \leq N_{\rm min} \leq 60$) and for seven values of the core radius $D_{\rm core}$ ($7\,h^{-1}$ Mpc $\leq D_{\rm core} \leq 10\,h^{-1}$ Mpc) using a linking length $l_{\rm link} = 5\,h^{-1}$ Mpc. The main results averaged over these $N_{\rm min}$ and $D_{\rm core}$ are listed in Table 2.

6.4.1 *'Galaxy' walls in real space*

In real space for all mock catalogues the parameters $\tau_{\rm v}$, $\langle h_{\rm w}\rangle$ and $\langle\epsilon_{\rm w}\rangle$ are similar to those found for the basic OCDM model. The velocity dispersion of 'galaxies' within walls, $\langle w_{\rm w}\rangle \approx \sigma_{\rm v} \approx \sigma_{\rm vel}$, exceeds that found for the basic model by about of 20–30 per cent. These variations can be attributed to the preferential identification of 'galaxies' in the central high-density regions of walls, where the relative velocities of DM particles are also larger than the mean values. The wall thickness and the velocity dispersion of 'galaxies' can be reduced and turned into dimensionless quantities in the same manner as in equation (6.4), and the PDFs for the reduced wall thickness and velocity dispersion within walls, N_ζ and N_ω, are also similar to Gaussian functions. The PDFs N_ω are shown in Fig. 5 for the mock$_4$ catalogue.

As expected, the mean surface density of walls, $\langle q_{\rm w}\rangle$, exceeds that found for the basic OCDM model, and this excess progressively increases, together with the biasing factor used. This excess can be considered as a suitable measure of the bias. This means that to characterize this bias the difference between $\tau_{\rm m}$ and $\tau_{\rm v}$ and/or between $\tau_{\rm m}$ and other amplitudes measured for the same catalogues can be used, together with the autocorrelation function. The growth of $q_{\rm w}$ leads to a proportional growth of δ, as the wall thickness is only weakly distorted.

The large-scale bias increases the contrast between richer and poorer walls, which is seen as an essential growth of the mean wall separation. In all mock catalogues, $\langle D_{\rm sep}\rangle$ is about 2 times larger than in the basic OCDM model. The growth of both $\langle q_{\rm w}\rangle$ and $\langle D_{\rm sep}\rangle$ does not distort the relation between $f_{\rm w}$ and $f_{\rm dq}$.

6.4.2 *'Galaxy' walls in redshift space*

In redshift space the fraction of the same particles assigned to walls in both real and redshift spaces becomes $f_{\rm cr} \sim 80$–85 per cent (Table 2), which explains the similarity of parameters $\langle q_{\rm w}\rangle$ and $\tau_{\rm m}$ listed in Table 2 for both cases. The expected growth of wall richness in redshift space according to (3.13) is not found, and the surface densities of walls, $\langle q_{\rm w}\rangle$, are, within the range of errors, the same in both real and redshift spaces. This fact shows that for 'galaxies' the expected growth of wall richness in redshift space is suppressed even more strongly than for DM component due to the relaxation of compressed matter. Then equation (3.1) describes correctly the time dependence of the mean wall surface density.

The parameters $\langle h_{\rm w}\rangle$ and $\langle w_{\rm w}\rangle$ for 'galaxy' walls are similar to those found for the underlying OCDM model. The difference of $\langle w_{\rm w}\rangle$ found for the same samples of walls in real and redshift spaces and a slow decrease of $\langle w_{\rm w}\rangle$ for the more strongly biased models can be assigned to the loss of a small fraction of particles with large velocities, which demonstrates the sensitivity of these functions to the method of wall identification.

In redshift space we have not which a reliable independent estimator of the amplitude as $\tau_{\rm v}$. There the bias is seen as a relation of the amplitudes $\tau_{\rm m} \geq \tau_{\xi}$. This makes it difficult to estimate quantitatively the relatively moderate large-scale bias in observed catalogues, because both $\tau_{\rm m}$ and τ_{ξ} are sensitive to the bias.

This discussion shows that the simple algorithm used in DMRT for the 'galaxy' identification does not significantly distort the basic characteristics of simulated walls, and a stronger bias can be seen as an excess of the surface density of 'galaxies' relative to that found for the DM component in the basic model. At the same time the mean velocity dispersions of both the DM component and the 'galaxies' assigned to walls, $\langle w_{\rm w}\rangle$, tend to be smaller than $\sigma_{\rm v}$ and $\tau_{\rm v}$, and other characteristics of the amplitude of perturbations.

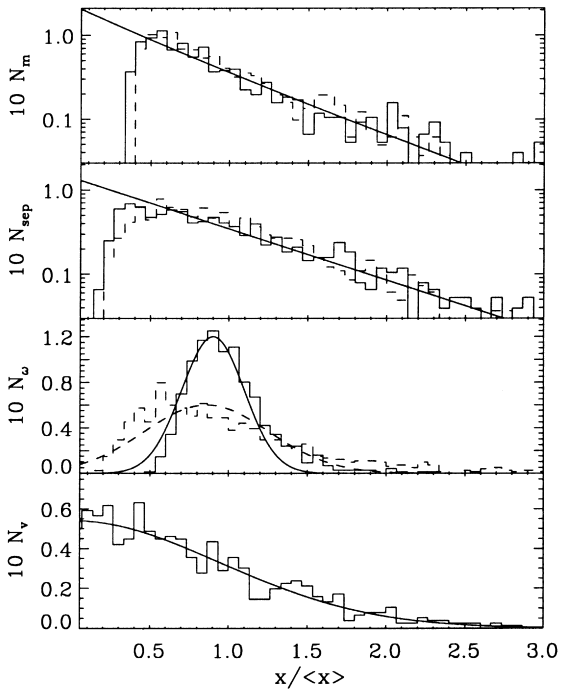

Figure 5. PDFs of wall surface density, $N_{\rm m}(q_{\rm w}/\langle q_{\rm w}\rangle)$, wall separation, $N_{\rm sep}(D_{\rm sep}/\langle D_{\rm sep}\rangle)$, reduced velocity dispersion, $N_{\omega}(\omega/\langle\omega\rangle)$, and velocity of walls, $N_{\rm v}(v_{\rm w}/\sigma_{\rm v})$, for the *mock*$_4$ catalogues in real (solid lines) and redshift (dashed lines) spaces. The same fits as in Figs 1–4 are plotted as well.

7 SUMMARY AND DISCUSSION

In this paper we continue the investigation of large-scale matter distribution and processes of large-scale structure formation and evolution. Some aspects of these problems were discussed in our previous papers (LCRS1; LCRS2; DURS; DMRT; Müller et al. 1998), where the 3D analysis of the observed and simulated large-scale structure was performed with the core-sampling and the Minimal Spanning Tree techniques. Another approach to this problem, based on the percolation technique, was discussed in Sahni, Sathyaprakash & Shandarin (1994), Sathyaprakash, Sahni & Shandarin (1998) and Shandarin & Yess (1998). The statistical description of structure formation and evolution based on the Zel'dovich theory of non-linear gravitational instability can be found in Lee & Shandarin (1998) and DD99.

Here we direct our attention to the physical aspects of the process of wall formation, which implies a more detailed discussion of the properties of DM walls in real space. The simulations described and investigated in DMRT are used to test the theoretical expectations, to estimate the influence of small-scale clustering and relaxation of compressed matter and other random factors, and to examine the power of the statistical methods used to describe the large-scale matter distribution. Three cosmological models, at different evolutionary stages, were analysed in the same manner, and the comparison of results obtained for these models allows us to estimate the properties of walls at various τ.

In redshift space the influence of small-scale clustering and large velocity dispersion of compressed matter noticeably distorts some characteristics of the walls. These distortions also appear in the considered mock catalogues, and can even be enhanced by the possible large-scale bias between the spatial distribution of DM and galaxies.

Some of these results may depend on the code used for the simulations (see, e.g., the discussion in Splinter et al. 1998), and they should be checked with simulations employing a code with higher spatial resolution.

7.1 Identification of walls

The core-sampling approach described in Section 5 allows us to characterize, in more detail, the matter distribution along the sampling core, and to estimate the uncertainty in measured properties of wall-like condensations introduced by the influence of velocity dispersion and small-scale clustering. The influence of these random factors is demonstrated by comparing results obtained with various $D_{\rm core}$, $N_{\rm min}$ and $l_{\rm link}$.

Results presented in Section 6 show that some fraction of the early compressed matter has subsequently evaporated due to relaxation processes. These DM particles, together with the infalling matter, form an extended halo around the walls, and it is therefore difficult to separate the walls from the background. The same problem is met by the correct definition of boundaries of galaxies and clusters of galaxies. It was also discussed by DMRT, LCRS2 and DURS, where the methods of wall selection, described in Section 6, were applied to simulated DM and observed galaxy distributions.

The central high-density part of walls is reliably selected in all

the cases, but various definitions of the wall boundaries can noticeably change the measured characteristics of walls. To provide more objective comparisons of wall characteristics, the same dimensionless parameters f_w and δ_{thr} should be used for identification of walls in different catalogues and simulations.

7.2 DM walls in real space

7.2.1 Measured characteristics of walls

The results presented in Section 6 show that the core-sampling approach can be successfully used for the investigation and description of the large-scale matter distribution and the wall-like matter condensations. It allows us to estimate the surface density, thickness, velocity dispersion and other basic parameters of DM walls corrected for the influence of random curvature and shape of walls. These parameters differ from those obtained in 3D space with the Minimal Spanning Tree and inertia tensor methods, and these methods suitably complement each other.

The measured wall characteristics can be compared with predictions of the Zel'dovich theory, which reveals the influence of relaxation of compressed matter on the properties of walls and allows us to correct the theoretical expectations. The small-scale clustering of compressed matter and the wall disruption lead to noticeable variations of measured wall characteristics for different parameters of the sampling core. These variations are not so large for the low-density models, but they increase rapidly with τ.

The dimensionless surface density of walls, q_w, is closely connected with the size of proto-walls as discussed by DMRT, LCRS2 and DURS. The high surface density of walls, $q_w \geq 0.6$, found above even for the low-density models, demonstrates that processes of strong non-linear matter evolution occur at a typical scale of $\sim q_w l_v \sim (15\text{–}25)\, h^{-1}$ Mpc. This evolution is correctly described by the Zel'dovich theory. This characteristic is sensitive to the basic cosmological parameters, Ω_m and h, which allows us to select the class of more perspective models for further investigation.

7.2.2 Relaxation of compressed matter

The problem of relaxation of compressed matter is now in the forefront, and the results obtained allow us to begin a discussion of the statistical characteristics of this relaxation. The analysis performed in real space is more important for the discussion of the basic physical processes which occurred during the formation of wall-like matter condensations, such as the small-scale matter clustering and the relaxation of the compressed matter. These processes generate the large velocity dispersion within walls and lead to the evaporation of high-velocity particles. Thus, in all these cases a significant deficit of energy in DM walls as compared with the expectations of the Zel'dovich theory –~(50–80) per cent and more–was found. The growth of this deficit with τ from the OCDM to SCDM models demonstrates that the DM relaxation becomes more and more important for later evolutionary stages, and its influence on the observed parameters of the large-scale matter distribution becomes crucial for $\tau \geq 0.5$.

The relaxation is seen in rich superclusters of galaxies such as the Perseus-Pisces supercluster (Saslaw & Haque–Copilah 1998). It is essentially accelerated and amplified by the small-scale clustering of compressed matter. This clustering is clearly seen in observations as, for example, a strongly inhomogeneous galaxy distribution within the Great Wall (Ramella et al. 1992). The clusters of galaxies situated within wall-like superclusters similar to the Great Wall and the Perseus-Pisces supercluster can be considered as extreme examples of this process.

The merging of structure elements formed earlier is very important for the formation of large walls (DD99). This means that actually the relaxation occurs step by step during all the evolutionary history, beginning with the formation of first low-mass, high-density pancakes which later are successively integrated and merged to larger structure elements. This means also that the finally reached degree of relaxation and the properties of compressed matter depend on the (unknown) evolutionary history of the considered walls, and therefore can be characterized only statistically.

The relaxation of compressed matter destroys the tight correlation between the surface density and velocity dispersion predicted by the Zel'dovich theory (3.6), but it generates other correlations between the same characteristics described by the relations (6.4). This fact indicates that the properties of compressed matter are sufficiently general, and these characteristics can be used to improve the methods of wall selection and the description of wall properties.

The velocity dispersion within walls increases gradually with τ from the OCDM to the SCDM model. As was discussed in Section 6, the particles with high velocity are gravitationally confined and occupy preferentially the high-density central regions of walls. This fact confirms that, these particles are probably relaxed and have a (quasi)stationary distribution. This distribution is not as stationary as, for example, that in clusters of galaxies, and it is slowly evolving due to the large-scale matter flow along the walls and the persisting merging of neighbouring structure elements, but presumably this evolution does not significantly distort the distribution of the formed matter.

7.3 DM walls in redshift space

The matter condensation seen in redshift space can be artificially enhanced partly by the influence of streaming velocities. The possible influence of this effect has been widely discussed over the past decade (see, e.g., Kaiser 1987, McGill 1990a, Davis, Miller & White 1997, Hamilton 1998 and Hui et al. 2000) and, as applied to properties of absorption lines in the spectra of high-redshift quasars, by McGill (1990b) and more recently by Levshakov & Kegel (1996, 1997). These tendencies are also clearly seen from the direct application of the Zel'dovich approximation to the wall formation in redshift space as was discussed in Section 3.2. Of course, it is impossible to decide which particles belong to walls, but we can estimate statistically the properties of DM walls identified in redshift space. However, the influence of this uncertainty cannot be separated from the influence of the relaxation and other factors discussed above.

For all models the comparison of DM walls selected in real and redshift spaces demonstrates that they are composed mainly from the same particles–this fraction is about $f_{cr} \sim (70\text{–}80)$ per cent (Table 2). This means that in both cases we find the same walls, and the fraction of randomly added or lost particles is indeed small. In spite of this, some properties of walls in redshift space are quite sensitive to the velocity dispersion and to the methods of wall identification. Thus the strong growth of wall thickness–about a factor of 2 – confirms results obtained by Melott et al. (1998). This effect is quite similar to the well-known 'finger of God' effect observed in clusters of galaxies.

The wall surface density, q_w, is most interesting, as it is directly connected with the basic cosmological parameters, Ω_m and h. Our analysis shows that for low-density models–ΛCDM and OCDM–the measured value of q_w is similar in both real and redshift spaces. This means that the growth of the matter condensation within walls due to streaming velocities as predicted by the Zel'dovich theory is strongly suppressed by the influence of the matter relaxation and the transformation of a continuous matter infall to a discontinuous one. Actually, similar relations connect the fundamental wall characteristics such as q_w and τ_m.

The velocity dispersion within walls selected in 3D redshift space can be noticeably underestimated, which is a direct consequence of the method of wall selection. In redshift space, particles with large velocities are artificially shifted to the periphery of selected walls, and so can be omitted from the analysis.

7.4 Walls in mock catalogues

For the considered mock catalogues the influence of velocity dispersion is enhanced by the methods used for 'galaxy' selection. The large-scale bias increases the 'galaxy' concentration within walls, and so increases the density gradient near the wall boundary. When the 'galaxies' are identified preferentially in the high-density central parts of the walls (in real space), then their velocity dispersion exceeds that for the DM particles, and this excess may be as large as ∼(20–30) per cent. In redshift space, the parameters of 'galaxy' walls such as $\langle h_w \rangle$ and $\langle w_w \rangle$ are similar to those in the underlying DM distribution.

The bias is clearly seen in both real and redshift spaces as an excess of the mean surface density of walls. The comparison of parameters q_w and τ_m found for observed wall-like galaxy condensations with possible independent estimates of the same parameters gives us a chance to obtain a reasonable observational estimates of the large-scale bias.

7.5 The amplitude of large-scale perturbations

These results demonstrate again that all characteristics of the amplitude and evolutionary stage of large-scale structure considered in Sections 2 and 3 are similar, but not identical, to each other, as they are sensitive to different properties of perturbations. The best and most stable measure, τ_v, comes from measurements of the velocity of structure elements. It is insensitive to the nonlinear evolution of perturbations, large-scale bias and small-scale clustering or relaxation of the compressed matter.

The comparison of other estimates for the same parameter τ, namely, τ_{vel}, τ_ξ, and τ_m obtained in the same simulations demonstrates their sensitivity to various natural and artificial factors. For the low-density models–ΛCDM and OCDM–the parameters τ_v and τ_m are usually sufficiently close to each other, which is a direct consequence of the close connection of the process of wall formation with the large-scale perturbations. The parameter τ_m is sensitive to a possible large-scale bias, but to reveal this factor, we need to have independent unbiased estimates of the same amplitude.

The most interesting independent estimate of the amplitude is τ_ξ, which is, however, more sensitive to small-scale matter clustering. Thus, for the SCDM model where this clustering is stronger it significantly overestimates the large-scale amplitude. It is less sensitive to the large-scale bias than τ_m.

Independent estimates of the large-scale amplitude come from measurements of the CMB anisotropy. The *COBE* data are consistent with other available estimates of cosmological parameters and of the large-scale amplitude, and therefore τ_T can be considered as the best estimate of the combination (2.9) of Γ and the amplitude. It can be connected with estimates of cosmological parameters $\Omega_m \approx 0.3$, $\Omega_\Lambda \approx 0.7$ obtained from observations of high-redshift supernovae (Perlmutter et al. 1998). None the less, τ_T should be corrected for a possible contribution of gravitational waves.

The investigation of the space density of clusters of galaxies and its redshift evolution (see, e.g., Bahcall & Fan 1998, Eke et al. 1998 and Wang & Steinhardt 1998) seems also to be promising and can give the required independent measure of the large-scale amplitude. The formation and evolution of galaxy clusters is caused by large-scale perturbations, and their characteristics can be connected with these perturbations. However, they are sensitive to the thermal evolution of clusters and, moreover, are related to only ∼(10–15) per cent of matter accumulated by the clusters. This means that they are not free from random variations, which are seen, in particular, as the well-known variations of the autocorrelation function with the cluster sample.

The critical discussion of available measurements of cosmological parameters (Efstathiou 1999; Wang et al. 1999) shows that, in spite of a large progress reached during recent years, we do not have yet a reliable unbiased estimate of these parameters, and these data should be tested with respect to possible random large-scale variations. The application of the methods discussed to large observed redshift surveys can help to achieve this goal.

ACKNOWLEDGMENTS

We are grateful to our anonymous referee for useful comments and criticism. This paper was supported in part by Denmark's Grundforskningsfond through its support for an establishment of Theoretical Astrophysics Center and Polish State Committee for Scientific Research grant Nr. 2-P03D-014-17. AGD also acknowledges support from the Center for Cosmo-Particle Physics 'Cosmion' in the framework of the project 'Cosmoparticle Physics'.

REFERENCES

Bahcall N. A., Fan X., 1998, ApJ, 504, 1
Bardeen J. M., Bond J. R., Kaiser N., Szalay A., 1986, ApJ, 304, 15 (BBKS)
Bond J. R., Kofman L., Pogosyan D., 1996, Nat, 380, 603
Bunn E. F., White M., 1997, ApJ, 480, 6
Buryak O., Doroshkevich A., Fong R., 1994, ApJ, 434, 24
Cannon R., 1998, in Müller V., Gottlöber S., Mücker J. P., Wambsganss J., eds, Large Scale Structure: Tracks and Traces. World Scientific, Singapore, p. 87
Cole S., Weinberg D. H., Frenk C. S., Ratra B., 1997, MNRAS, 289, 37
Cole S., Hatton S., Weinberg D. H., Frenk C. S., 1998, MNRAS, 300, 945
Coles P., Melott A., L ., Shandarin S. F., 1993, MNRAS, 260, 765
Colless M. M., 1998, Phil. Trans. R. Soc. London A, 357, 105
Davis M., Miller A., White S. D. M., 1997, ApJ, 490, 63
de Lapparent V., Geller M. J., Huchra J. P., 1988, ApJ, 332, 44
Demiański M., Doroshkevich A., 1999a, ApJ, 512, 527
Demiański M., Doroshkevich A., 1999b, MNRAS, 306, 779 (DD99)
Doroshkevich A. G., Tucker D. L., Oemler A., Kirshner R. P., Lin H., Shectman S. A., Landy S. D., Fong R., 1996, MNRAS, 283, 1281 (LCRS1)

Doroshkevich A. G., Tucker D. L., Lin H., Turchaninov V., Fong R., 1999a, MNRAS, preprint TAC 1997-031, submitted (LCRS2)
Doroshkevich A. G., Müller V., Retzlaff J., Turchaninov V. I., 1999b, MNRAS, 306, 575 (DMRT)
Doroshkevich A., Fong R., McCracken G., Ratcliffe A., Shanks T., Turchaninov V. I., 2000, MNRAS, 315, 767 (DURS)
Efstathiou G., 1999, MNRAS, 310, 842
Eke V. R., Cole S., Frenk C. S., Henry J. P., 1998, MNRAS, 298, 1145
Giovanelli R., Haynes M. P., 1993, AJ, 105, 1271
Governato F. et al., 1998, Nat, 392, 389
Hamilton A. J. S., 1998, in Hamilton D., ed., The Evolving Universe. Kluwer, Dordrecht, p. 185
Hui L., Kofman L., Shandarin S. F., 2000, ApJ, 537, 12
Jenkins A. et al., 1998, ApJ, 499, 20
Kaiser N., 1987, MNRAS, 227, 1
Lee J., Shandarin S., 1998, ApJ, 500, 14
Levshakov S. A., Kegel W. H., 1996, MNRAS, 278, 497
Levshakov S. A., Kegel W. H., 1997, MNRAS, 288, 787
Loveday J., Pier J., 1998, in Colombi S., Mellier Y., Raban B., eds, Wide Field Surveys in Cosmology. Editions Frontières, p. 317, astro-ph/9809179
McGill C., 1990a, MNRAS, 242, 428
McGill C., 1990b, MNRAS, 242, 544
Melott A. L., Coles P., Feldman H. A., Wilhite B., 1998, ApJ, 496, L85
Müller V., Doroshkevich A. G., Retzlaff J., Turchaninov V. I., 1998, in Giuricin G., Mezzetti M., Salucci P., eds, Observational Cosmology: The Development of Galaxy Systems, Sesto 1998. Astron. Soc. Pac., San Francisco, p. 297
Oort J. H., 1983, ARA&A, 21, 373
Oort J. H., 1984, A&A, 139, 211
Peebles P. J. E., 1993, Principles of Physical Cosmology. Princeton Univ. Press, Princeton
Perlmutter S. et al., 1999, ApJ, 517, 565
Ramella M., Geller M. J., Huchra J. P., 1992, ApJ, 384, 396
Ratcliffe A., Shanks T., Broadbent A., Parker Q. A., Watson F. G., Oates A. P., Fong R., Collins C. A., 281, L47
Sahni V., Sathyaprakash B. S., Shandarin S. F., 1994, ApJ, 431, 20
Saslaw W. C., Haque–Copilah S., 1998, ApJ, 509, 595
Sathyaprakash B. S., Sahni V., Shandarin S. F., 1998, ApJ, 508, 551
Shandarin S., Yess 1998, ApJ, 505, 12
Shandarin S., Zel'dovich Ya.B., 1989, Rev. Mod. Phys., 61, 185
Shectman S. A. et al., 1996, ApJ, 470, 172
Splinter R. J., Melott A. L., Shandarin S. F., Suto Y., 1998, ApJ, 497, 38
Steidel C. C., Giavalisco M., Pettini M., Dickinson M., Adelberger K. L., 1996, ApJ, 462, L17
Tadros H., Ballinger W. E., Taylor A. N. et al., 1999, MNRAS, 305, 527
Wang L., Steinhardt P. J., 1998, ApJ, 508, 483
Wang L., Cardwell R. R., Ostriker J. P., Steinhardt P. J., 2000, ApJ, 530, 17
Zel'dovich Ya.B., 1970, A&A, 5, 20
Zel'dovich Ya.B., 1978, in Longair M., Einasto J., eds, Proc. IAU Symp. 79, Large Scale Structure in the Universe. Reidel, Dordrecht, p. 409

APPENDIX A: DYNAMICAL CHARACTERISTICS OF WALLS IN THE ZEL'DOVICH THEORY

The results obtained in DD99 allow us to discuss in more details dynamical characteristics of walls predicted in the Zel'dovich theory. The comparison of these expected and actually simulated characteristics reveals the influence of interaction and relaxation of compressed matter.

Following DD99 we define the wall formation as the intersection of two DM particles with different Lagrangian coordinates, $\boldsymbol{q}_1$ and $\boldsymbol{q}_2$. The difference of these coordinates measures the size of the pancake. Using the basic relations of the Zel'dovich theory (2.2) and (2.3), linking the Lagrangian and Eulerian coordinates and velocities of particles, we obtain the coordinate and velocity of a wall as a whole (DD99):

$$r_{\rm w} = \frac{1}{l_{\rm v} q_{\rm w}} \int_{q_1}^{q_2} \mathbf{nr} dq = \frac{l_{\rm v}}{1+z}\left(q_{\rm c} - \tau(z)\frac{\Delta\Phi}{q_{\rm w}}\right),$$

$$v_{\rm w} = \frac{1}{l_{\rm v} q_{\rm w}} \int_{q_1}^{q_2} \boldsymbol{n}[\boldsymbol{u} - H\boldsymbol{r}] dq$$

$$= \frac{l_{\rm v} H(z)}{1+z}\left[q_{\rm c} - \tau(z)(1+\beta)\frac{\Delta\Phi(q_{\rm w})}{q_{\rm w}}\right],$$

$$\boldsymbol{n} = \frac{\boldsymbol{q}_1 - \boldsymbol{q}_2}{|\boldsymbol{q}_1 - \boldsymbol{q}_2|}, \quad q_{\rm c} = \frac{|\boldsymbol{q}_1 + \boldsymbol{q}_2|}{2 l_{\rm v}}, \quad q_{\rm w} = \frac{|\boldsymbol{q}_1 - \boldsymbol{q}_2|}{l_{\rm v}}, \tag{A.1}$$

where $\Delta\Phi(q_{\rm w})$ is the random difference of the dimensionless gravitational potential over the wall. It is convenient to introduce the relative normalized Lagrangian coordinate of a particle within a wall, ϑ:

$$q_{\rm p} = q_{\rm c} + 0.5 q_{\rm w}\vartheta, \quad -1 \le \vartheta \le 1.$$

Using the coordinate ϑ we will describe the relative position and velocity of the infalling particle with the Lagrangian coordinate $q_{\rm p}$ or ϑ by the functions:

$$r_{\rm inf} = \mathbf{nr} - r_{\rm w} = \frac{l_{\rm v}}{1+z}\left[\frac{q_{\rm w}}{2}\vartheta - \tau(z)\left(S(\vartheta) - \frac{\Delta\Phi(q_{\rm w})}{q_{\rm w}}\right)\right],$$

$$v_{\rm inf} = \mathbf{nv} - v_{\rm w} = -u(z) 0.5 q_{\rm w}\vartheta + H(z)(1+\beta) r_{\rm inf},$$

$$u(z) = H(z) l_{\rm v} \beta(z) (1+z)^{-1}. \tag{A.2}$$

Here $S = \boldsymbol{nS}$ is thee random dimensionless longitudinal displacement of a particle from its unperturbed Lagrangian position introduced by (2.2).

For Gaussian initial perturbations the PDF of the random function $r_{\rm inf}$ is also Gaussian, and the mean value and dispersion of $r_{\rm inf}$ should be found using the conditional characteristics of functions S and $\Delta\Phi$ taking into account that a wall is formed in the point $r = r_{\rm w}$ (DD99). In this case for walls with $q_{\rm w} < 1$ we have:

$$\langle r_{\rm inf}\rangle \approx \frac{l_{\rm v}}{1+z}\frac{q_w^3}{4}\vartheta \ll \sqrt{\langle r_{inf}^2\rangle} \approx \frac{l_{\rm v}\tau(z)}{1+z}\sqrt{\frac{q_{\rm w}}{3}}, \tag{A.3}$$

and $\langle r_{inf}^2\rangle$ is independent from ϑ. This means that both random functions,

$$r_{\rm inf} \text{ and } v_{\rm inf} + u(z) 0.5 q_{\rm w}\vartheta = H(z)(1+\beta) r_{\rm inf}$$

are also independent from ϑ. Hence, for the thickness, $h_{\rm w}$, of a wall with the surface density $q_{\rm w}$, and for the velocity dispersion within such a wall we have

$$h_w^2 = 12 \times \frac{1}{2}\int_{-1}^{1} d\vartheta \langle r_{inf}^2\rangle = 4 l_v^2 \tau^2 q_{\rm w} (1+z)^{-2}, \tag{A.4}$$

$$w_w^2 = \frac{1}{2}\int_{-1}^{1} d\vartheta \langle v_{inf}^2\rangle = \frac{H^2 l_v^2}{(1+z)^2}\left(\frac{\beta^2}{12} q_w^2 + \frac{\tau^2(1+\beta)^2}{3} q_{\rm w}\right).$$

Here the wall thickness is normalized by the thickness of a homogeneous slice.

This paper has been typeset from a TEX/LATEX file prepared by the author.